



Forschungszentrum Karlsruhe
in der Helmholtz-Gemeinschaft

Wissenschaftliche Berichte
FZKA 7312

Magnetohydrodynamic Flow in a Mock-Up of a HCLL Blanket. Part I Numerical Analysis

C. Mistrangelo

Institut für Kern- und Energietechnik
Programm Kernfusion

September 2008

Forschungszentrum Karlsruhe

in der Helmholtz Gemeinschaft

Wissenschaftliche Berichte

FZKA 7312

**Magnetohydrodynamic flow in a mock-up
of a HCLL blanket. Part I Numerical analysis**

C. Mistrangelo

Institut für Kern- und Energietechnik
Programm Kernfusion

Forschungszentrum Karlsruhe GmbH, Karlsruhe
2008

Für diesen Bericht behalten wir uns alle Rechte vor

Forschungszentrum Karlsruhe GmbH
Postfach 3640, 76021 Karlsruhe

Mitglied der Hermann von Helmholtz-Gemeinschaft
Deutscher Forschungszentren (HGF)

ISSN 0947-8620

urn:nbn:de:0005-073129

Magnetohydrodynamic flow in a mock-up of a HCLL blanket

Abstract

A modular *Helium Cooled Lead Lithium* (HCLL) blanket concept has been proposed to be tested in the first phase of ITER operation as part of the Test Blanket Module (TBM) program of the European Union. In this blanket concept helium is used to cool the breeder zones through cooling plates immersed in the liquid metal as well as the whole structure (first wall and grid plates). The liquid breeder circulates in the rectangular gaps formed by the cooling plates inside the breeder units and only a small velocity (1 – 1.5 mm/s) is required to direct it towards external facilities for tritium removal and purification of the liquid metal. The interaction of the moving lead lithium with the strong magnetic field that confines the plasma induces electric currents, which create electromagnetic forces. These latter modify the velocity and pressure distributions compared to those in hydrodynamic flows. Since all the walls, cooling and grid plates, are electrically conducting, an exchange of electric currents through common walls of adjacent fluid domains may lead to an electric flow coupling and its effects on the flow and pressure distribution have to be investigated. The detailed knowledge of the established magnetohydrodynamic (MHD) flow is required to assess the reliability of this blanket design.

In the present report results from a numerical study of MHD flows in four breeder units with internal cooling plates are discussed. The geometric features are chosen according to the characteristics of the experimental test section that is inserted in the liquid metal loop of the MEKKA laboratory at the Forschungszentrum Karlsruhe for the 2007-2008 experimental campaign. The analysis focuses on the effects of electric coupling between adjacent breeder units. Results have been obtained for a pure toroidal magnetic field and for cases where the field has a certain inclination with respect to the toroidal direction.

In the case of a pure toroidal magnetic field, velocity jets develop close to the grid plates and a small increase of the velocity is also observed near the cooling plates. The electric coupling between breeder units is weak since currents do not cross the grid plates, but they flow preferentially in tangential direction within the walls separating the boxes. Instead, inside the breeder units, the narrow ducts formed by the cooling plates are strongly coupled.

It has been found that the presence of a poloidal component of the confining magnetic field yields a stronger electric coupling between the breeder units and more complex current paths can be identified.

This MHD study has been initiated to advance our understanding of the proposed HCLL blanket concept, to identify the main MHD issues for this design and to define further R&D areas to be investigated as part of the ongoing experimental program at the Forschungszentrum Karlsruhe.

Magnetohydrodynamische Strömung im Modellexperiment eines HCLL Blankets

Zusammenfassung

Im Europäischen Fusionsprogramm sind Tests eines modularen Helium-gekühlten Bleilithiumblankets vorgesehen, die in der ersten Versuchsphase von ITER durchgeführt werden. In diesem Blanketkonzept werden die Kühlplatten der Brutzone sowie die gesamte Struktur (First Wall, Grid Plates) mit Helium gekühlt. Zur Tritiumabfuhr und Reinigung des Flüssigmetalls in externen Anlagen zirkuliert das Brutmaterial PbLi mit Geschwindigkeiten von 1 – 1.5 mm/s in rechteckförmigen Kanälen zwischen den Kühlplatten der Bruteinheiten. Durch die Wechselwirkung des bewegten Bleilithiums mit dem starken Magnetfeld, das das Plasma einschließt, werden elektrische Ströme induziert. Die hieraus resultierenden elektromagnetischen Kräfte verändern die Geschwindigkeits- und Druckverteilung im Vergleich zu hydrodynamischen Strömungen. Da es möglich ist, dass die Strömungen in benachbarten Flüssigmetallgebieten durch den Austausch elektrischer Ströme durch leitende Trennwände miteinander gekoppelt sind, müssen diese Effekte untersucht werden. Eine genaue Kenntnis der magnetohydrodynamischen (MHD) Strömung ist zur Beurteilung der Zuverlässigkeit dieses Blankets erforderlich.

In diesem Bericht werden Ergebnisse einer numerischen Studie diskutiert, in der MHD Strömungen in vier Bruteinheiten mit internen Kühlplatten untersucht werden. Die Geometrie entspricht der experimentellen Teststrecke, die für die Versuchskampagne 2007-2008 im MEKKA Labor des Forschungszentrums Karlsruhe eingebaut ist. Die Berechnungen konzentrieren sich auf die Effekte der elektrischen Kopplung zwischen benachbarten Bruteinheiten. Es werden Ergebnisse für den Fall eines toroidalen Magnetfeldes vorgestellt sowie Ergebnisse für Magnetfelder mit einer gewissen Neigung bezüglich der toroidalen Richtung.

Für den Fall eines reinen toroidalen Magnetfeldes entstehen Geschwindigkeitsjets in der Nähe der Grid Plates und leichte Geschwindigkeitsüberhöhungen in der Nähe der Kühlplatten. Die elektrische Kopplung zwischen Bruteinheiten ist schwach, da elektrische Ströme nicht durch die Grid Plates hindurch treten. Sie fließen hauptsächlich tangential entlang dieser Wände, die die Einheiten voneinander trennen. Im Gegensatz hierzu sind die engen Fluidbereiche zwischen den Kühlplatten einzelner Bruteinheiten stark miteinander gekoppelt.

Falls eine zusätzliche poloidale Komponente des Magnetfeldes vorhanden ist, kommt es zu einer stärkeren Kopplung zwischen den Bruteinheiten und man findet dann kompliziertere elektrische Stromspfade.

Diese Arbeit soll zu einem besseren Verständnis des vorgeschlagenen Konzepts eines Helium-gekühlten PbLi Blankets beitragen, die MHD Probleme dieses Designs aufzeigen und weiterführende Arbeiten definieren, die in zukünftigen theoretischen und experimentellen Programmen des Forschungszentrums untersucht werden.

Magnetohydrodynamic flow in a mock-up of a HCLL blanket

Part I Numerical analysis

Contents

1	Introduction	1
2	Formulation of the problem	3
2.1	Governing equations and boundary conditions	3
2.2	Electric potential as flow streamfunction	4
3	Numerical model	6
4	Experimental test section	6
5	Results and discussion	10
5.1	Toroidal magnetic field	10
5.1.1	Current density and electric potential	10
5.1.2	Velocity	18
5.2	Toroidal-poloidal magnetic field	20
5.2.1	Current density and electric potential	20
5.2.2	Velocity	22
5.2.3	Current and velocity distribution without cooling plates	25
5.2.4	Effects of increasing the poloidal field component	26
5.3	Poloidal magnetic field	30
5.3.1	Electric potential and current density	30
5.3.2	Velocity	32
6	Comparison with experimental data	33
7	Conclusions	36
8	Further required investigations	38
	References	39

1 Introduction

Different blanket concepts have been selected to be tested in the first phase of ITER operation. These designs have to provide adequate performance when extrapolated to a fusion reactor power plant.

The blanket is the mechanical structure that surrounds the plasma in fusion reactors. It has several functions: it absorbs the high energy neutrons transforming their kinetic energy into heat, which is then transferred to the coolant. The blanket acts also as a shield preventing neutrons from reaching the superconducting magnets. In addition this component ensures the breeding of tritium necessary to fuel the reactor. In order to accomplish this task, the blanket should contain a breeder material having at least some fraction of lithium. Attractive candidates are liquid metal alloys, e.g. the eutectic PbLi, due to their high tritium breeding capability and their large thermal conductivity. Moreover, they offer tritium self-sufficiency without the need of an additional neutron multiplier.

In the blanket liquid metals can be used both as coolant and breeder (*self-cooled concepts*) or exclusively to produce tritium (*separately cooled blankets*) like in the *Helium Cooled Lead Lithium* (HCLL) blanket design. Here the liquid metal is employed only as breeder and the total heat is removed by helium. The separately cooled blanket concepts have the advantage that the liquid metal can be circulated inside the blanket at much smaller velocity than in the self-cooled designs. As a consequence, the pressure drop caused by the magnetohydrodynamic interaction between the flowing PbLi and the strong magnetic field that confines the plasma should not be a critical feasibility issue at least in the breeder units.

A partial view of the current HCLL blanket concept (Rampal, Gatelet, Giancarli, Laffont, Li-Puma, Salavy and Rigal (2006)) is shown in Fig.1. It is a modular design, where grid plates (GPs) are used to form a frame of rectangular cells, called breeder units (BUs), in which cooling plates (CPs) are inserted. The liquid metal is used only as breeder and the total heat is removed by helium flowing at high velocity and pressure within channels integrated in all the walls and in the cooling plates. Each column of breeder boxes is fed with liquid metal through a poloidal manifold, then the fluid enters the BUs by flowing through narrow vertical gaps in the back plate and expands in the flat sub-channels formed by cooling plates. These fluid domains have a high aspect ratio (ratio of toroidal width to the poloidal height) that can affect and modify the velocity distribution compared to the case of an almost square duct. A number of five cooling plates in each breeder unit has been considered in this design to remove the volumetrically released fusion power and to keep the wall temperature below critical values. The BUs are connected two by two at the first wall via a small opening through which the PbLi passes from one box to the adjacent one before being collected into a second poloidal manifold.

In the BUs the liquid metal flows very slowly with velocities of the order of 1 – 1.5 mm/s. This weak circulation is required for tritium removal and for the purification of the liquid metal in which activation products (e.g. Po and Bi) and other impurities may be present (Boccaccini, Giancarli, Janeschitz, Hermsmeyer, Poitevin, Cardella and Diegele (2004)). The HCLL design requires a limited extrapolation of the present

technological knowledge and for this reason it is regarded as a promising candidate for being tested in ITER.

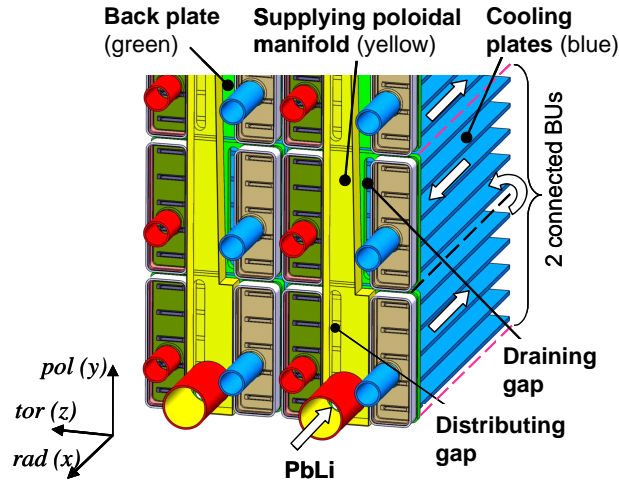


Figure 1: Partial view of two adjacent columns of breeder units (rectangular boxes whose grid plates are indicated by dash lines). The supplying poloidal manifold is displayed in yellow and the cooling plates in blue. The turning arrow indicates the connection at the first wall between two BUs .

Since the velocity distribution close to the walls governs the tritium permeation and the transfer processes for heat and corrosion products, the flow redistribution due to MHD effects is an important issue for this design. It must be verified for instance that no excessive corrosion occurs and regions with high accumulation of tritium have to be avoided since they could increase tritium permeation losses up to unacceptable values.

The attractiveness of this blanket is strongly related to the possibility of controlling and predicting the MHD phenomena caused by the interaction of the flowing liquid metal with the magnetic field (Morley, Malang and Kirillov (2005)). Some of these MHD issues will be discussed and analyzed in the present report. They involve the MHD flow in high aspect ratio channels that are fully electrically coupled to adjacent flow domains, and the investigation of the effect of a magnetic field not aligned with the walls (cooling and grid plates) of the breeder units.

Computations of MHD flow in the prototypical 3D geometry given by the design, consisting of a single breeder unit without internal cooling plates, part of the supplying poloidal manifold and the feeding circular pipe, have been performed by Bühler (2005) by means of asymptotic numerical techniques.

Additional studies are required to investigate the influence of the cooling plates on current and velocity distribution and to check if there is an homogeneous partition of the liquid metal in the flat ducts formed by the cooling plates. Moreover, since in this blanket all the walls are electrically conducting, an exchange of currents through the common dividing walls may lead to an electric coupling of the flow in

neighboring channels. This phenomenon, known as multichannel effect, modifies the velocity distribution compared to that in separated ducts.

The MHD flow in assemblies formed by three electrically connected ducts coupled at walls perpendicular to the applied magnetic field has been studied by McCarthy and Abdou (1991). Fully developed liquid metal flow in three rectangular ducts coupled at walls parallel to the magnetic field has been instead investigated by Molokov (1993) by using an asymptotic solution.

2 Formulation of the problem

2.1 Governing equations and boundary conditions

The equations for the steady state laminar, incompressible, viscous, MHD flow are written in dimensionless form so that the relative importance of the forces acting on the flow can be inferred by the size of multiplying non-dimensional groups. These dimensionless equations describe conservation of momentum, mass and charge, with current density given by Ohm's law:

$$\frac{1}{N} (\mathbf{v} \cdot \nabla) \mathbf{v} = -\nabla p + \frac{1}{Ha^2} \nabla^2 \mathbf{v} + \mathbf{j} \times \mathbf{B}, \quad (1)$$

$$\nabla \cdot \mathbf{v} = 0, \quad \nabla \cdot \mathbf{j} = 0, \quad (2)$$

$$\mathbf{j} = -\nabla \phi + \mathbf{v} \times \mathbf{B}. \quad (3)$$

By taking the divergence of (3) and using charge conservation, a Poisson equation for the electric potential is obtained:

$$\nabla^2 \phi = \nabla \cdot (\mathbf{v} \times \mathbf{B}) = \mathbf{B} \cdot \boldsymbol{\omega}, \quad (4)$$

which states that the electric potential is determined by the component of the flow vorticity along magnetic field direction, namely by the variation of the velocity components in a plane perpendicular to \mathbf{B} .

In these equations the variables \mathbf{v} , \mathbf{B} , \mathbf{j} , p and ϕ denote the velocity, the applied magnetic field, the current density, the pressure and the electric potential, scaled by the reference quantities v_0 , B_0 , $\sigma v_0 B_0$, $\sigma v_0 B_0^2 L$ and $v_0 B_0 L$, respectively. Here the half width of a breeder unit, measured along the toroidal direction, is chosen as characteristic length L and the velocity scale v_0 corresponds to the average velocity in the cross-section of a breeder unit. The quantity B_0 is the magnitude of the applied magnetic field. The fluid properties like the electric conductivity σ , the kinematic viscosity ν , and the density ρ are assumed to be constant.

The problem is solved supposing that for small magnetic Reynolds numbers ($Re_m = \mu \sigma L v_0 \ll 1$, where μ is the magnetic permeability) the magnetic field induced by currents in the fluid is negligible compared to the imposed one. Therefore, the main interaction between the electromagnetic field and the moving fluid is associated with the appearance of the electromagnetic force $\mathbf{j} \times \mathbf{B}$. Hydrodynamic

equations and Maxwell's equations are coupled by the Lorentz force and the induced electric field $\mathbf{v} \times \mathbf{B}$ present in Ohm's law.

The flow is governed by two non-dimensional groups, the Hartmann number and the interaction parameter

$$Ha = B_0 L \sqrt{\frac{\sigma}{\rho \nu}}, \quad N = \frac{\sigma L B_0^2}{\rho v_0}. \quad (5)$$

The square of the Hartmann number characterizes the ratio of electromagnetic to viscous forces while the interaction parameter represents the ratio of electromagnetic to inertia forces.

In the present study the walls of the assembly have finite thickness t_w and electric conductivity σ_w and therefore part of the current flowing in the fluid may close its path in the walls. For that reason, the following equations are solved simultaneously in the solid domain:

$$\mathbf{j}_w = -\frac{\sigma_w}{\sigma} \nabla \phi_w, \quad \nabla \cdot \mathbf{j}_w = 0. \quad (6)$$

As boundary conditions at the fluid-wall interface the no-slip condition ($\mathbf{v} = 0$) is applied, together with conservation of wall-normal component of current density ($j_n = j_{nw}$) and continuity of electric potential ($\phi = \phi_w$). The surrounding medium is assumed to be insulating so that the normal component of the electric current vanishes at the outer surface of the external wall.

2.2 Electric potential as flow streamfunction

Let us consider Ohm's law (3), which allows expressing the velocity components perpendicular to the homogeneous magnetic field $\mathbf{B} = B \hat{\mathbf{z}}$ as

$$\mathbf{v}_\perp = \frac{1}{B} \left(-\frac{\partial \phi}{\partial y} - j_y \right) \hat{\mathbf{x}} + \frac{1}{B} \left(\frac{\partial \phi}{\partial x} + j_x \right) \hat{\mathbf{y}} \quad (7)$$

This expression shows that the local velocity is determined by the potential gradient and by the currents induced in the fluid. Since the electric current density \mathbf{j} for fully developed, high Hartmann number MHD flows in insulating ducts or in ducts with thin conducting walls ($c \ll 1$) is typically of the order $O(c + Ha^{-1}) \ll 1$, it should be negligible in the Ohm's law (3) in comparison with the terms of order unity, i.e. the potential gradient $\nabla \phi$ and the induced electric field $\mathbf{v} \times \mathbf{B}$. This fact permits to simplify expression (7) so that the velocity \mathbf{v}_\perp can be determined as

$$\mathbf{v}_\perp = u \hat{\mathbf{x}} + v \hat{\mathbf{y}} \approx -\frac{1}{B^2} (\nabla \phi \times \mathbf{B}) = -\frac{1}{B^2} \nabla \times (\phi \mathbf{B}) = \frac{1}{B} \left(-\frac{\partial \phi}{\partial y} \hat{\mathbf{x}} + \frac{\partial \phi}{\partial x} \hat{\mathbf{y}} \right). \quad (8)$$

Assuming the magnitude of the magnetic field B equal one, the previous expression reduces to:

$$\mathbf{v}_\perp = u \hat{\mathbf{x}} + v \hat{\mathbf{y}} \approx -\nabla \times (\phi \hat{\mathbf{z}}). \quad (9)$$

Therefore, the electric potential can be regarded as a stream function for the velocity field. It can be used to visualize streamline patterns, i.e. trajectories of fluid

particles. Since streamlines are tangent to the velocity vector of the flow, the value of a streamfunction is constant along a streamline. Therefore, lines along which $\phi = \text{const}$ represent streamlines of the flow field.

In plane flow, the difference between the stream function values at any two points in the considered fluid domain, i.e. the difference in stream function on two streamlines, gives the volumetric flow rate through the line connecting the two points.

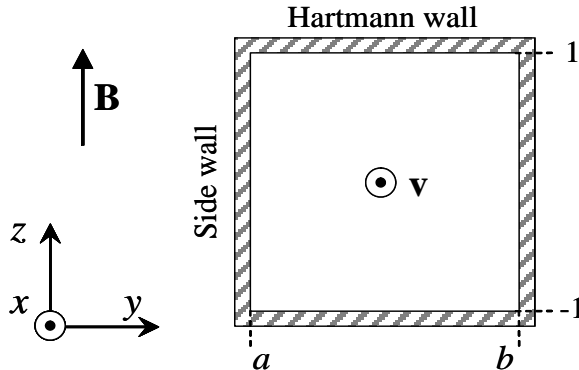


Figure 2: Channel geometry and orientation of the magnetic field.

The total flow rate Q in a duct is obtained by integrating the velocity over its cross section. Considering the channel in Fig.2, it can be written as

$$Q = \int_{-1}^1 \int_a^b u \, dy \, dz.$$

From (7) we have that the axial velocity u is given by the transverse potential gradient $-\partial\phi/\partial y$, therefore the volumetric flow rate can be written as

$$Q = \int_{-1}^1 \int_a^b -\frac{\partial\phi}{\partial y} \, dy \, dz = \int_{-1}^1 [\phi_a - \phi_b] \, dz. \quad (10)$$

The fraction of flow rate Q_c carried by the uniform core is determined analogously as

$$Q_c = \int_{-1}^1 \int_a^b u_c \, dy \, dz = \int_{-1}^1 [\phi_{c,a} - \phi_{c,b}] \, dz. \quad (11)$$

Since the core potential does not vary along magnetic field lines, the values at positions a and b equal the potentials at the Hartmann wall, i.e. $\phi_c = \phi(z = 1) = \phi_{H_{a,w}}$. As a result, the portion of flow transported by the side layers that develop at walls parallel to the magnetic field is obtained as

$$Q_s = Q - Q_c.$$

and the one carried by the single layer at position a becomes

$$Q_s = \int_1^{-1} [\phi_a - \phi_c] \, dz = \int_1^{-1} [\phi_{s,w} - \phi_{H_{a,w}}] \, dz, \quad (12)$$

namely, the flow rate in the side layer is obtained by integrating along magnetic field direction the difference between the potential on the side wall and the value at the Hartmann wall:

The utility of the electric potential as stream function lies in the fact that the velocity components in a plane perpendicular to the magnetic field at a specified point are given by the partial derivatives of the stream function at that point. Therefore, in experiments potential measurements on the surface of the test section can be usefully performed in order to obtain accurate and reproducible data for the stream function and therefore for the velocity field in the studied geometry.

3 Numerical model

The present investigation is carried out using the commercial package CFX-5.6, which is based on the finite volume method and on a modified form of the SIMPLE algorithm for pressure-velocity coupling to ensure mass conservation (Patankar (1980)). The discrete system of linearized equations is solved by an iterative procedure.

Since magnetohydrodynamic equations are not available as an option in CFX-5, these equations have been implemented in the code by means of Fortran subroutines. In order to describe MHD flows it is necessary to introduce the Lorentz force as a body force in the momentum equation and to solve a Poisson equation for the electric potential. The implementation of MHD equations in CFX has been described by Mistrangelo (2005).

Another aspect that has to be carefully considered in CFD simulations is the mesh used to discretize the computational domain. It is important to resolve properly the geometric features that affect the flow and the regions where the largest gradients of the variables occur, such as the boundary layers that develop along the walls. By increasing the Hartmann number, namely the magnetic field strength, the thickness of the boundary layers decreases. Therefore the need of resolving adequately these layers, while preserving the mesh quality, leads to a progressive rise in the total number of nodes. As a consequence, restrictions on the accuracy of the solution at high Hartmann numbers are related to limitations in the memory storage and computer capabilities.

Convergence of the solution is judged both by considering the value of the residuals of velocity and mass conservation and by monitoring the solution variables in fixed points of the computational domain during the run. Values of interest are, for instance, the maximum velocity in the side layers close to the grid and the cooling plates, and the potential difference between the walls parallel to the magnetic field. The calculations of MHD flows are stopped when all the root mean square residuals are equal or less than 10^{-5} and the variables at the monitored locations remain constant.

4 Experimental test section

Since a complete theoretical description for the HCLL blanket modules involving all the combined issues does not exist, an experiment has been designed in which a mock-up of a HCLL blanket is inserted in the liquid-metal NaK loop of the MEKKA laboratory at the Forschungszentrum Karlsruhe (Bühler, Brinkmann, Horanyi and Starke (2008)). Due to the limited space in the uniform magnetic field available in the magnet the test section is scaled by a factor two compared to the original TBM design (Rampal, Li-Puma, Poitevin, Rigal, Szczepanski and Boudot (2005)).

The used NaK loop provides a liquid metal inventory of about 200 l and the fluid is circulated by mechanical and electromagnetic pumps that allow reaching flow rates up to 25 m³/h and pressure heads up to 9 bar. A gyrostatic- and an electromagnetic flow meter are used to measure the flow rate. The transverse homogeneous magnetic field in which the test section is placed has a maximum value of 2.1 T in a volume of 170 × 480 × 800 mm³. A detailed description of the MEKKA facility can be found in a report by Barleon, Mack and Stieglitz (1996).

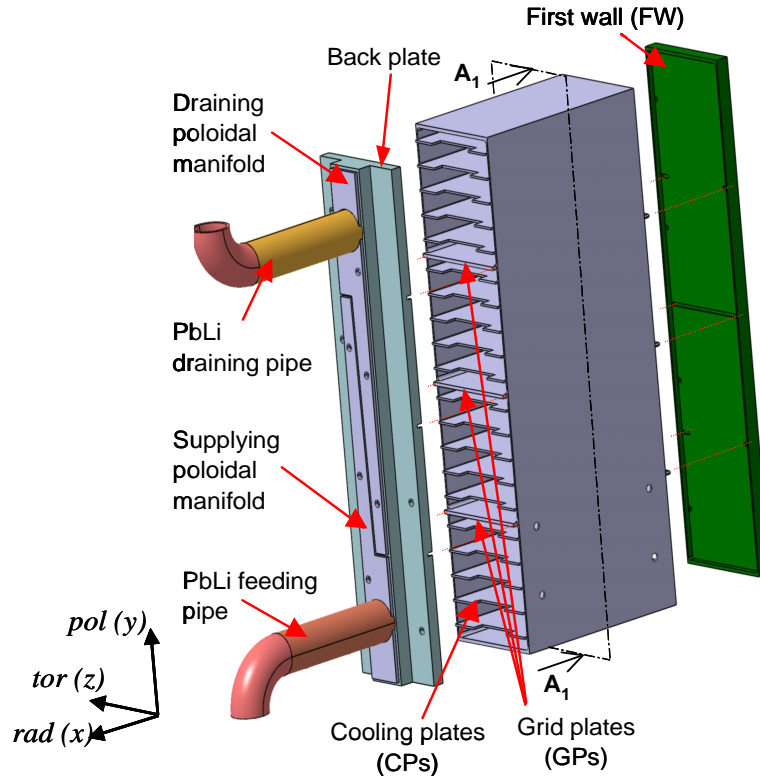


Figure 3: Assembly of the experimental TBM mock-up. The dash-dot line represents a cross-sectional plane A_1A_1 , at half distance from the back plate and the first wall, where the velocity and current distributions are analyzed numerically.

A view of the assembly used for the experimental campaign is shown in Fig.3. The test section consists of four breeder units separated by electrically conducting

grid plates. This is the minimum number of boxes that allows studying the pressure drop and flow behavior in the poloidal manifolds.

This can be clarified by considering the schematic representation of the experimental mock-up in Fig.4a. The feeding poloidal manifold (yellow) supplies the liquid metal to the breeder units 1 and 3 and the draining manifold (green) collects the fluid from the breeder units 2 and 4. Therefore at least 4 breeder units are required to investigate the NaK flow in the manifolds. A complete liquid metal path in the blanket module occurs instead in two breeder units. It starts in the feeding circular pipe, then the NaK expands in the supplying manifolds and it enters BU 1 (3) through a narrow gap in the back plate. The liquid metal distributes among the cooling plates and flows into the connected BU 2 (4) by passing in an opening near the first wall (Fig.4b). After distributing into the second BU the fluid is collected in the draining poloidal manifold. A circular pipe transports the liquid metal outside the blanket module.

For the MHD analysis different flow arrangements have to be considered: the co-current flow in the slender channels in each breeder unit and the counter-current flow in ducts, belonging to two different BUs, separated by a grid plate.

In the experimental mock-up, walls, which have internal helium channels in the original HCLL blanket modules, are designed as solid walls. Their thickness is reduced according to their steel content, namely it is scaled depending on the volume fraction of helium that flows in the channels integrated in the walls, in order to achieve in a first approximation an average electric conductance similar to that in the proposed design.

The working fluid in the loop is the eutectic sodium potassium alloy $\text{Na}^{22} \text{K}^{78}$. Due to its high electric conductivity ($\sigma_{NaK} = 2.88 \cdot 10^6 \text{ } (\Omega\text{m})^{-1}$ at 20°C) and low density ($\rho_{NaK} = 868.2 \text{ kg m}^{-3}$ at 20°C) (Foust (1972)), the experiments can be run in a range of parameters close to that relevant for fusion applications, while using magnetic fields that are about three times smaller than those in fusion reactors. Moreover, owing to its low melting point, the liquid metal loop can be operated at room temperature.

During the experiments, we are interested to measure the surface potential along the walls of the test section and in particular on those perpendicular to the magnetic field, called Hartmann walls. These data will serve as an indication of the flow distribution in the test section since, according to Ohm's law, the electric potential can be interpreted as velocity streamfunction.

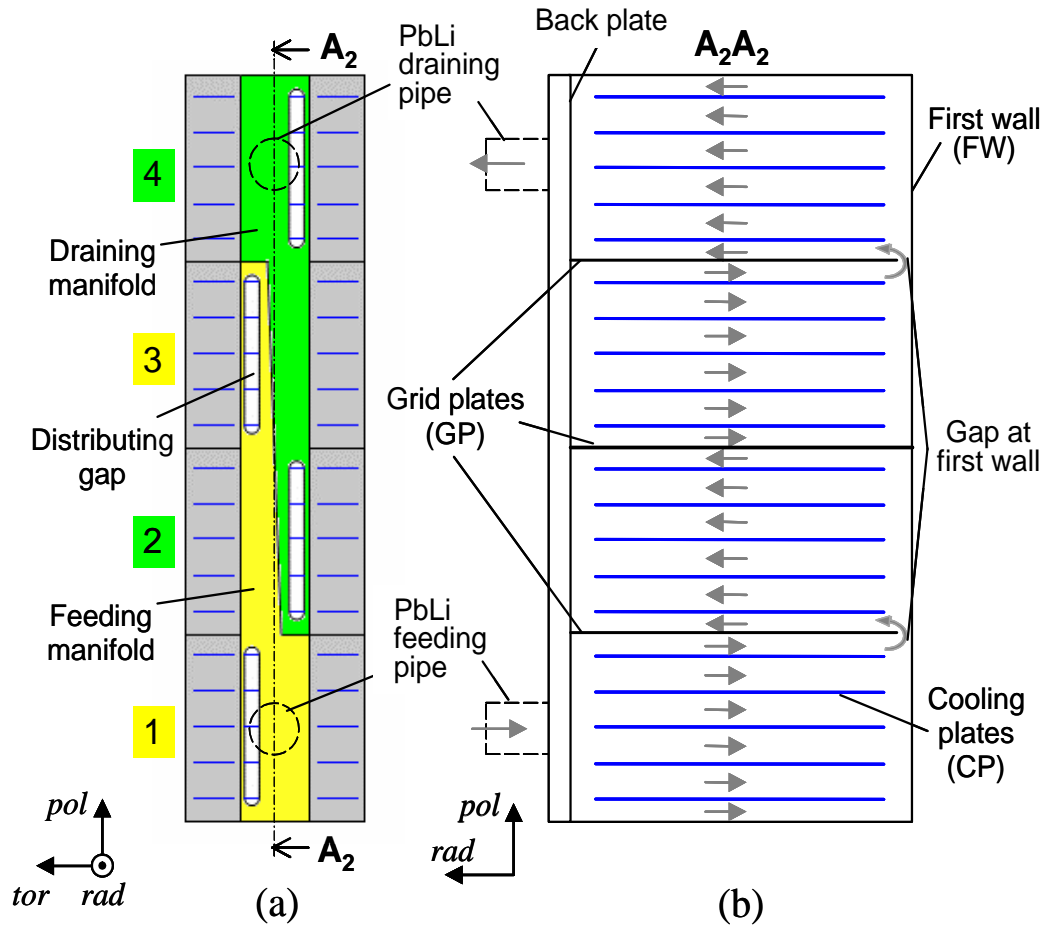


Figure 4: Schematic representation of the experimental test section. (a) The feeding poloidal manifold (yellow) supplies the liquid metal to breeder units 1 and 3. The draining manifold (green) collects the fluid from breeder units 2 and 4. (b) The vertical $rad - pol$ cut A_2A_2 shows the layout of the liquid metal flow path.

5 Results and discussion

In the following the results for multichannel MHD flows in geometries relevant for the study of the HCLL blanket are discussed. It is assumed that inside the breeder units, at certain distance from the manifolds (back plate) and from the first wall, fully developed conditions are established. Results are obtained both considering a pure toroidal applied magnetic field and fields with a given inclination with respect to the toroidal direction. The assumption of a fully developed flow in a middle cross section of the breeder units has been confirmed by first experiments performed for strong magnetic fields (Bühler et al. (2008)).

5.1 Toroidal magnetic field

Let us consider first the flow in four breeder units exposed to a toroidal magnetic field, which is parallel to cooling and grid plates, called side walls, and perpendicular to the walls that separate columns of breeder units, named Hartmann walls. The BUs as well as the internal flat ducts are electrically coupled at common side walls.

5.1.1 Current density and electric potential

The flow in adjacent breeder units is driven by applied constant pressure gradients of opposite sign and therefore, in neighboring boxes, the main stream is reversed. As a result, electric currents are induced in different directions according to the sign of the pressure gradients. Instead, in each BU, in the six sub-channels formed by the cooling plates, the liquid metal flows in the same direction. As a consequence, the electric currents in all the six slender ducts have the same orientation, as shown in Fig.5a. The red arrows indicate schematically the main current circulation.

The currents induced in the high aspect ratio ducts cross the cooling plates and couple strongly the flow in those channels. Consequently, as described later in Sect.5.1.2 (Fig.12), the velocity distribution between the cooling plates, in the four domains with equal aspect ratio, is the same. Instead in the grid plates and in the external side walls the current flows preferentially in tangential direction. This creates a parabolic potential distribution along the walls, as shown in Fig.10, that leads to an increased velocity in the layers at these side walls compared to that at the cooling plates. Moreover, there is no exchange of currents between adjacent breeder units across the common dividing wall, i.e. the electric coupling between the boxes is weak. This results from concomitant facts: the imposed magnetic field is purely toroidal, the BUs are coupled at side walls and the liquid metal in the boxes moves in such a way that a counter-current flow occurs at the grid plates.

This electric current distribution can be properly described by considering the topology of the current vector field in the walls, i.e. the position of singular points. Figure 5b describes how the currents flowing toroidally in the grid plate enter the Hartmann wall and split into two parts moving poloidally upward and downward. This change of direction of the currents from the toroidal to the poloidal one is indicated by the presence of a half saddle point at the external surface of the Hartmann

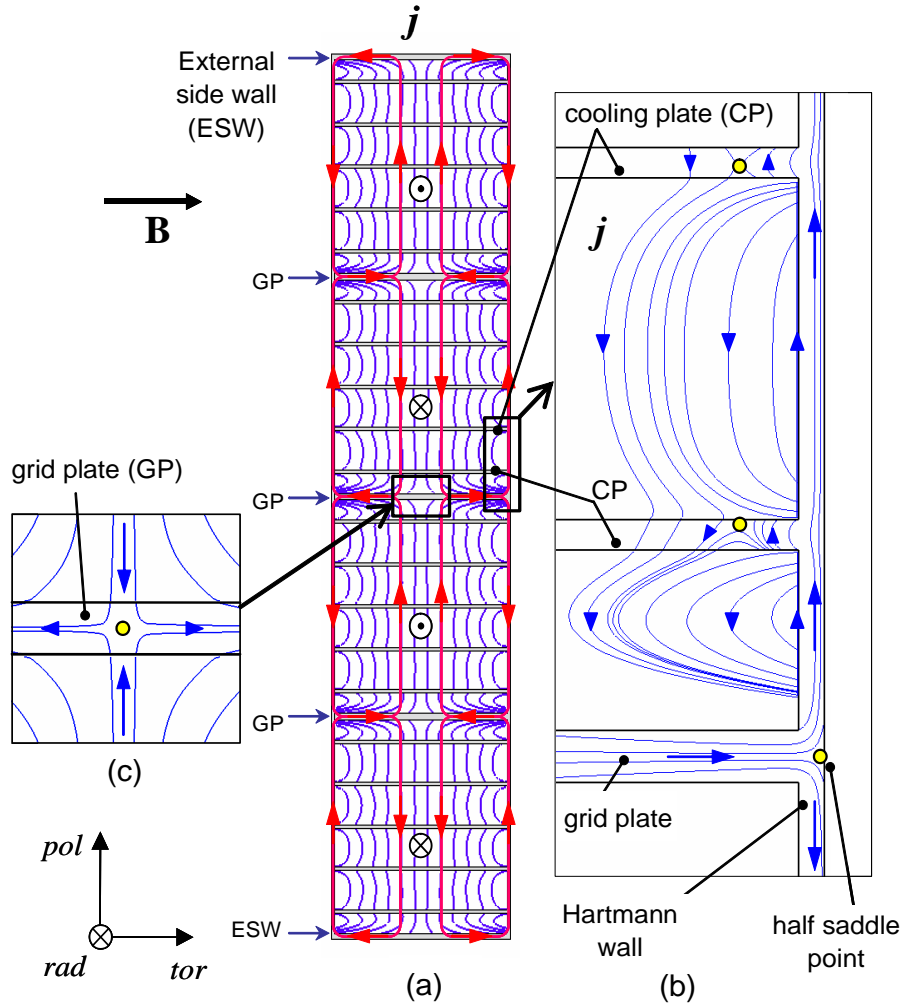


Figure 5: (a) Current streamlines in the BUs for $Ha = 3000$ and pure toroidal magnetic field. In each BU the flow direction is indicated. Detailed views show the characteristic points (yellow dots) produced by the current vector field, which appear (c) in the grid plates (GPs), and (b) in the Hartmann wall and in the cooling plates (CPs).

wall, at the intersection with the grid plate (yellow dot in Fig.5b). The variation of the location of this point will be useful to describe the modifications the current distribution undergoes when, in a next step, a magnetic field with an additional poloidal component ($B_{pol} \neq 0$) is applied.

The characteristic of the electric connection between breeder units, namely the above mentioned weak coupling, can be deduced by considering the current distribution in the grid plates, near the vertical symmetry plane (Fig.5c). Here a saddle point is present and the electric current distributes around it symmetrically with respect to both the poloidal and the toroidal axis. This indicates that the currents induced in two BUs enter the common dividing wall and flow parallel to it towards the Hartmann walls without crossing the grid plate.

In Fig.6 the patterns of the current streamlines for the cases with and without cooling plates are compared. The presence of the internal side walls in the BUs gives rise to a deformation of the current paths close to the Hartmann walls, perpendicular to the magnetic field. The currents flowing poloidally in these walls tend to enter the cooling plates. This leads to the appearance of saddle points near the Hartmann walls as shown in the details of Fig.6b. In the central cooling plate, in the middle of each box, the critical point is located at half of the wall thickness (Fig.6b2). In the other cooling plates the singularity is shifted towards one side of these internal walls. It can be observed that the arrangement of these characteristic points in a breeder unit is symmetric with respect to the central cooling plate.

The presence of the cooling plates leads to the appearance, inside each flat channel, of current loops that close mainly through the Hartmann layers and partially in the Hartmann walls without connecting electrically the internal ducts (Fig.7).

In Fig.8 the component j_z of the current density in magnetic field direction is plotted along the poloidal coordinate y at various toroidal z locations. It shows how j_z increases in the side layers that develop at the walls parallel to the magnetic field and becomes negligible in the cores of the internal channels where the current flows parallel to the Hartmann walls. Moreover, it can be noted that the magnitude of the current in the boundary layers along the grid plates is larger than the one in the layers near the external side walls. This can be explained considering that, since one grid plate belongs to two BUs, only half of its thickness contributes to its effective electrical conductance that results being smaller than the one of the external side walls. In other words, they have a higher resistance and therefore a larger amount of current induced in the fluid will close its path through the side layers rather than in the walls. This can be seen in Fig.8 where the maximum j_z near the GPs is higher than at the ESWs. Considering the magnitude of the total current density, this is one in the core of the flat ducts and it becomes larger while approaching the external and the internal side walls. Higher values are present near the grid plates. By moving closer to the Hartmann walls (e.g. curve at $z = 0.95$) the toroidal component of the current density rises strongly in a region near the corners of the flat ducts, in the side layers along cooling plates. This is due to the before described occurrence of current loops that close exclusively in the slender channels, and to the redistribution around the saddle points of current in the CPs (compare Fig.6b).

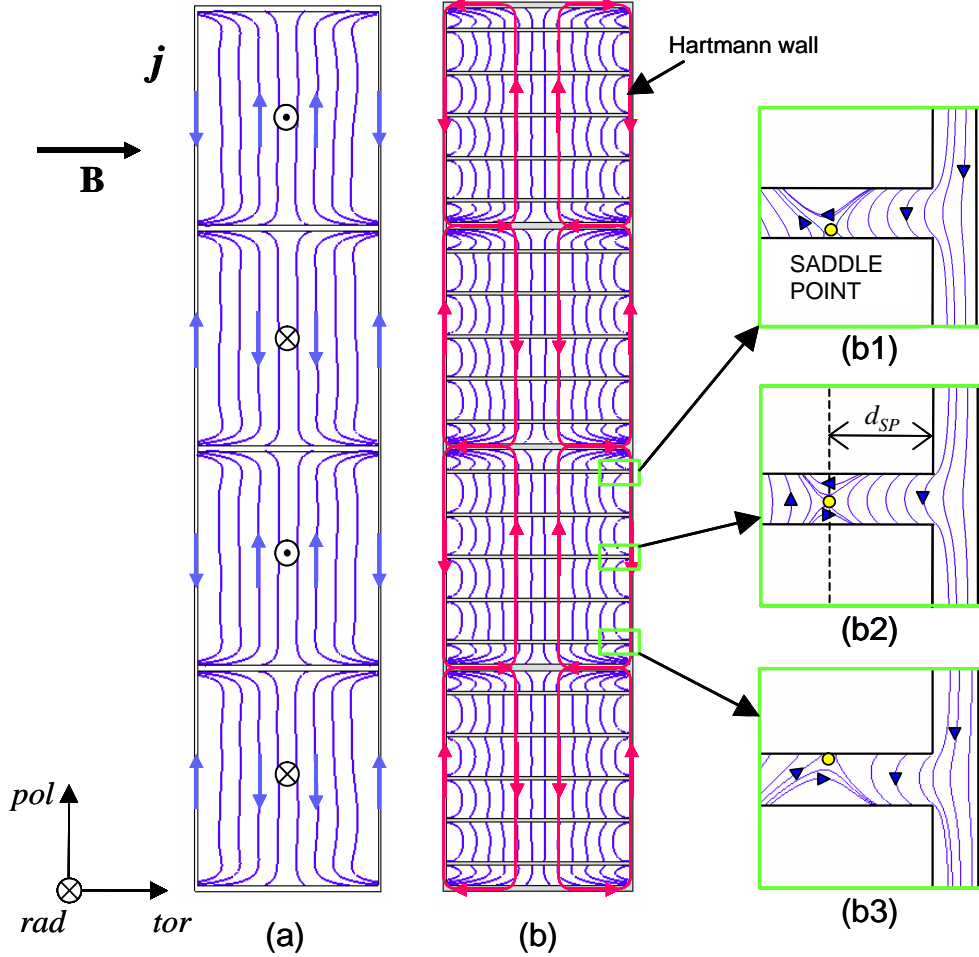


Figure 6: Current streamlines in four breeder units (a) without and (b) with internal cooling plates, for $Ha = 3000$ and pure toroidal magnetic field. Figure (b) shows detailed views of the deformation of current streamlines, near Hartmann walls, due to the presence of cooling plates and the appearance of singularities (yellow dots). The distance d_{SP} of the critical points in the CPs from the Hartmann wall corresponds to the toroidal extent of a region, near the duct corners, where a local maximum velocity is observed.

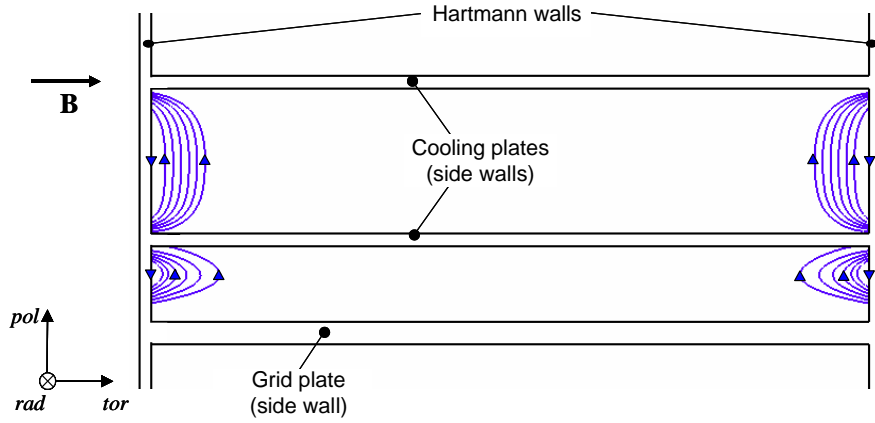


Figure 7: Current loops that close inside the narrow channels through the Hartmann layers and walls, for $Ha = 3000$ and toroidal magnetic field. They appear due to the presence of cooling plates.

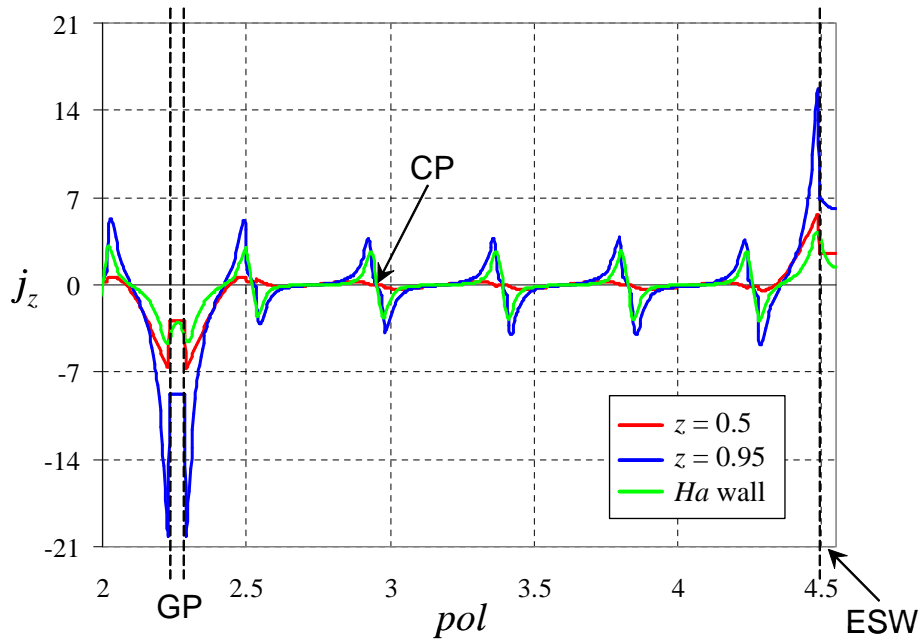


Figure 8: Component of the current density aligned with the magnetic field plotted as a function of the poloidal coordinate at various toroidal z positions, for $Ha = 3000$. GP, CP and ESW indicates a grid, a cooling plate and an external side wall, respectively.

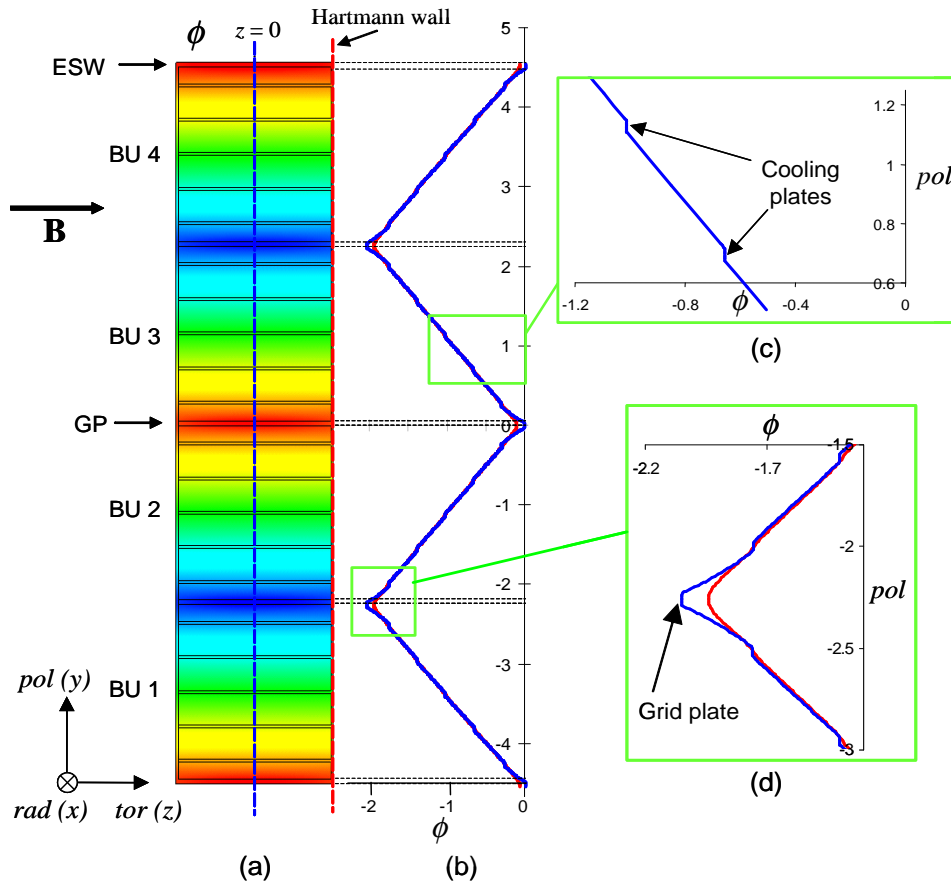


Figure 9: (a) Contours of calculated electric potential in the cross section of the experimental mock-up for $Ha = 3000$ and toroidal magnetic field. (b) The potential is plotted as a function of the poloidal direction along a line at $z = 0$ (blue curve) and along the Hartmann wall (red). The enlarged view shows that (c) the potential varies linearly in the flat ducts and it is constant across the cooling plates, and (d) deviations from the linear law are present near the grid plates and external side walls where currents flow preferentially in tangential direction.

Figure 9a displays the electric potential distribution in the four breeder units. In Fig.9b the potential is plotted as a function of the poloidal coordinate along the lines in the middle of the assembly at $z = 0$ (blue curve) and along the Hartmann wall (red line). It is observed that the potential varies linearly in the flat channels that form the breeder units. This fact suggests a uniform velocity distribution in these high aspect ratio ducts. Instead across the cooling and grid plates the potential is almost constant (Fig.9c).

By comparing the potential profiles on the symmetry plane ($z = 0$) and on the Hartmann wall it can be noted that in the cores of the ducts having larger aspect ratio the potential is almost the same, i.e. it does not vary in magnetic field direction. Instead at the grid plates and at the external side walls the magnitude of the potential

on the outer surface perpendicular to the magnetic field is smaller than on the central plane as highlighted in Fig.9d. The difference between the two curves is related to the flow rate carried by the boundary layers along these side walls, as explained in the following.

Along magnetic field lines the electric potential is almost constant in the cooling plates, which behave as being perfectly electrically conducting, and it has a parabolic distribution in the external side walls and in the grid plates where most of the current flows tangentially to the wall. Moreover, as it has been already observed, the core potential is uniform along magnetic field lines. As a result a potential difference is present across the side layer that produces flow rates transported by high velocity jets at these side walls. Figure 10 displays the electric potential profile along the central grid plate of the mock-up, having taken as a reference value the potential in the middle point of the assembly at $y, z = 0$.

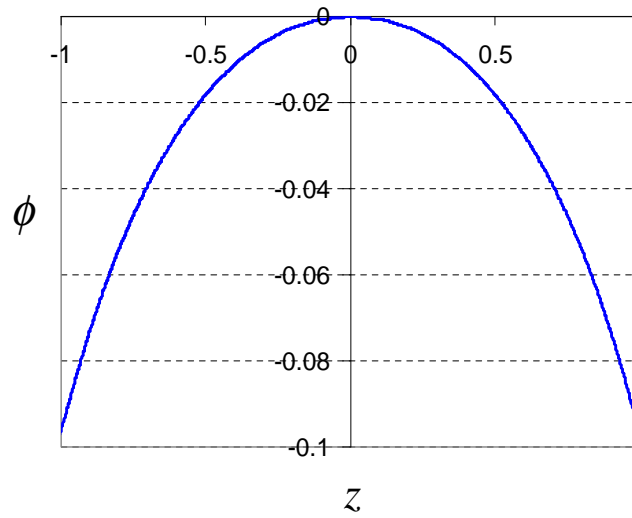


Figure 10: Electric potential as a function of the toroidal coordinate, plotted along the central grid plate of the test section, for $Ha = 3000$ and toroidal magnetic field. The potential in the middle of the geometry at $y, z = 0$ has been considered as a reference value.

As described in Sect.2.2 the potential can be regarded as a flow streamfunction and it can give information about flow rate. More precisely, the integral of the difference between the potential along a side wall and the correspondent value on the Hartmann wall represents the flow rate transported by the layer that develops along the considered parallel wall. In Fig.11 this difference is plotted as a function of the toroidal direction z along a grid plate (red curve) and an external side wall (green profile). It shows that the flow rate at the internal side wall is higher than at the external one. This can be explained for instance in terms of current flowing inside the parallel walls and layers. An external side wall and a grid plate have almost the same thickness and therefore equal resistance but, in the latter one a larger current

flows coming from two boxes. This results in a higher potential difference along a grid plate compared to that at an external side wall. The difference between the integrals of the two curves plotted in Fig.11 gives the value of the additional mass flow rate in the side layers along the grid plates compared to that at the external side walls. This quantity is related to the difference between the maxima of the two parabolic profiles. These maximum values are clearly visible in Fig.9b-d by comparing the potential distributions along the symmetry plane and at the Hartmann wall. Therefore, as mentioned above, the deviation between these curves can be related to the mass flow rate carried by the parallel layers.

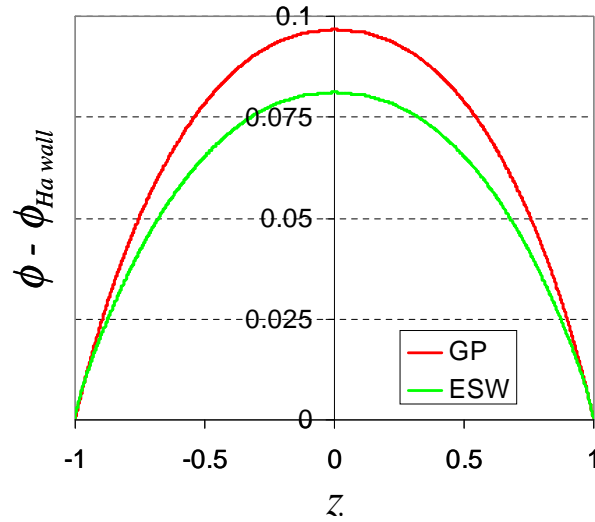


Figure 11: Potential distribution reduced by the value of the potential on the Hartmann wall, $\phi_{Ha\ wall}$, plotted along a grid plate (GP) and an external side wall (ESW), for $Ha = 3000$ and toroidal magnetic field.

As a consequence of the particular distribution of current and potential, the velocity in the side layers along cooling plates increases when approaching the Hartmann walls. The local maximum of the velocity in these boundary layers is observed in a zone whose toroidal extent corresponds to the distance d_{SP} of the singularity from the Hartmann wall (Fig.6b 2). The complete description of velocity distribution is given in details in the next section (see Fig.12).

5.1.2 Velocity

Some of the features of the velocity distribution in the mock-up have been already anticipated in the previous sections. In the following the main characteristics are recalled and further details are given.

Figure 12a shows contours of radial velocity in the breeder units. Larger values are present at the grid plates and at the external side walls, in the boundary side layers that develop at the walls parallel to the imposed magnetic field.

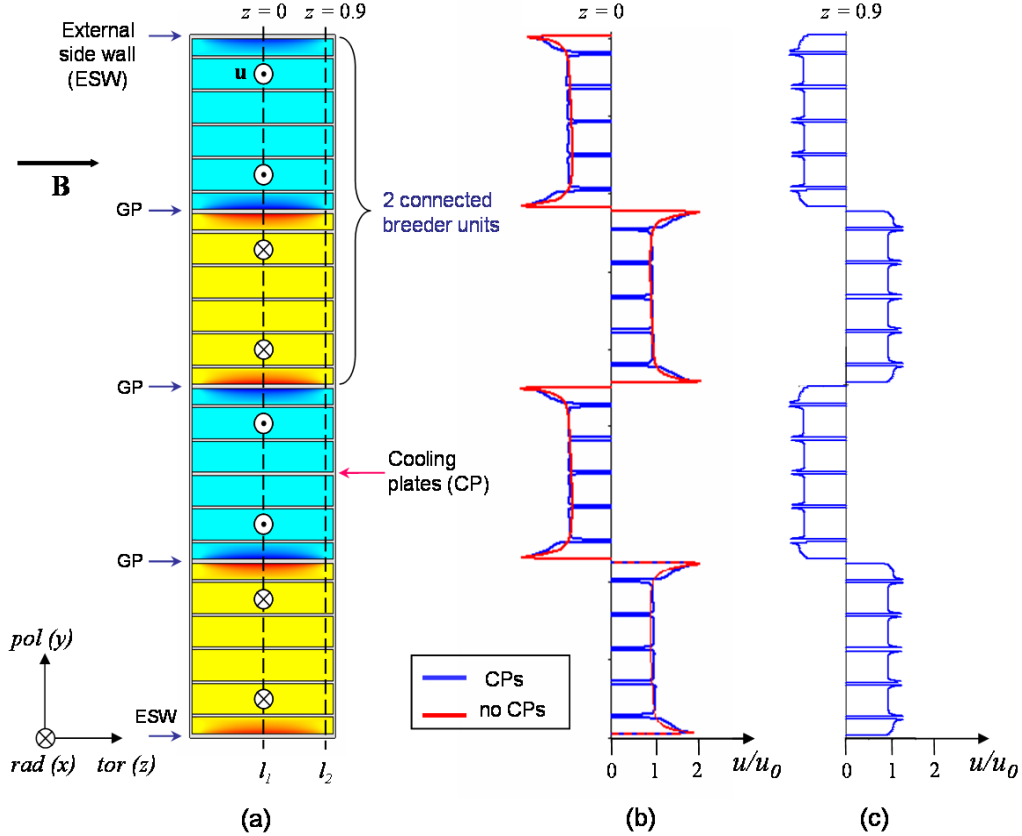


Figure 12: (a) Contours of radial velocity in four BUs with cooling plates, for $Ha = 3000$ and toroidal magnetic field. The non-dimensional radial velocity is plotted (b) along a line at $z = 0$, in the middle of the assembly, for the cases with (blue line) and without (red line) cooling plates, and (c) along the line at $z = 0.9$, near the Hartmann wall.

Near the grid plates the velocity and the side layer flow rate are slightly higher than those at the external side walls. As already pointed out during the discussion of current and potential distribution, this larger flow rate can be explained both in terms of reduced effective conductance of the grid plates compared to that of the external side walls or considering the larger current flowing in the internal walls. As a result there is a smaller potential variation along the external side walls and a

weaker influence on the velocity profile in the parallel layers. This is shown in Fig.13 where the toroidal potential gradient $\partial\phi/\partial z$ is plotted along an internal grid plate (GP) and an external side wall (ESW).

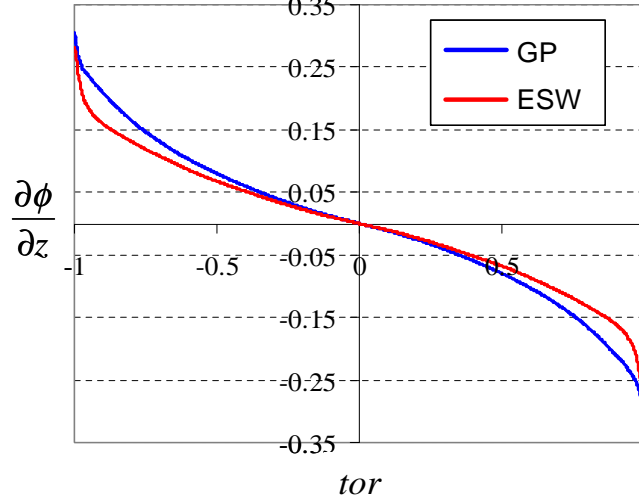


Figure 13: Toroidal potential gradient along a grid plate (GP) and an external side wall (ESW), for the case $Ha = 3000$ and pure toroidal magnetic field.

At the cooling plates only a small increase of the velocity is observed since the current enters these internal side walls mainly in perpendicular direction. Therefore, the cooling plates have the same effect on the flow as if they were perfectly conducting. This results in a strong electric coupling of the flow in the sub-channels that form a breeder unit.

The main flow features are well described by Fig.12b where the non dimensional radial velocity is plotted as a function of the poloidal direction along the line at $z = 0$. In the cores of the ducts with same aspect ratio a flat uniform velocity distribution is observed, with a small increase at the cooling plates, as expected for channels having perfectly conducting side walls. In each BU the most external ducts, at top and bottom of the box, have a higher aspect ratio and side walls of different thickness and therefore different electrical conductance. As a result, in those channels the two side layers at the walls parallel to \mathbf{B} merge and no uniform core region occurs any more. The red curve instead represents the velocity profile obtained when omitting the cooling plates in the BUs. The comparison of the results for the two cases with and without CPs shows the weak effect of these internal walls on the flow distribution.

As mentioned during the discussion of current distribution (Sect.5.1.1, Fig.6), the presence of a toroidal current component near the junctions between cooling plates and Hartmann walls leads to a local increase of the velocity close to the internal side walls. This is shown in Fig.12c, where the radial velocity is plotted along the line at $z = 0.9$.

5.2 Toroidal-poloidal magnetic field

The previous results were obtained for a pure toroidal magnetic field. However, in the blanket an additional poloidal component is required to confine the plasma. Therefore, in general the resulting magnetic field is not aligned with the walls (cooling and grid plates) of the breeder units. In the following the results for the case of magnetic field inclined with respect to the toroidal direction are discussed. The detailed velocity distribution in the breeder units depends on the angle of inclination of the magnetic field, namely on the value of the poloidal component, B_{pol} . Nevertheless, the main flow features described for $B_{pol} = 0.1B_{tor}$ are similar also in the cases with a larger poloidal component of the magnetic field.

5.2.1 Current density and electric potential

Figure 14a shows the contour plots of the electric potential for $Ha = 3000$ and $B_{pol} = 0.1B_{tor}$ and indicates that the solution for potential as well as the one for velocity, as will be described later, is inclined along the direction of the imposed magnetic field.

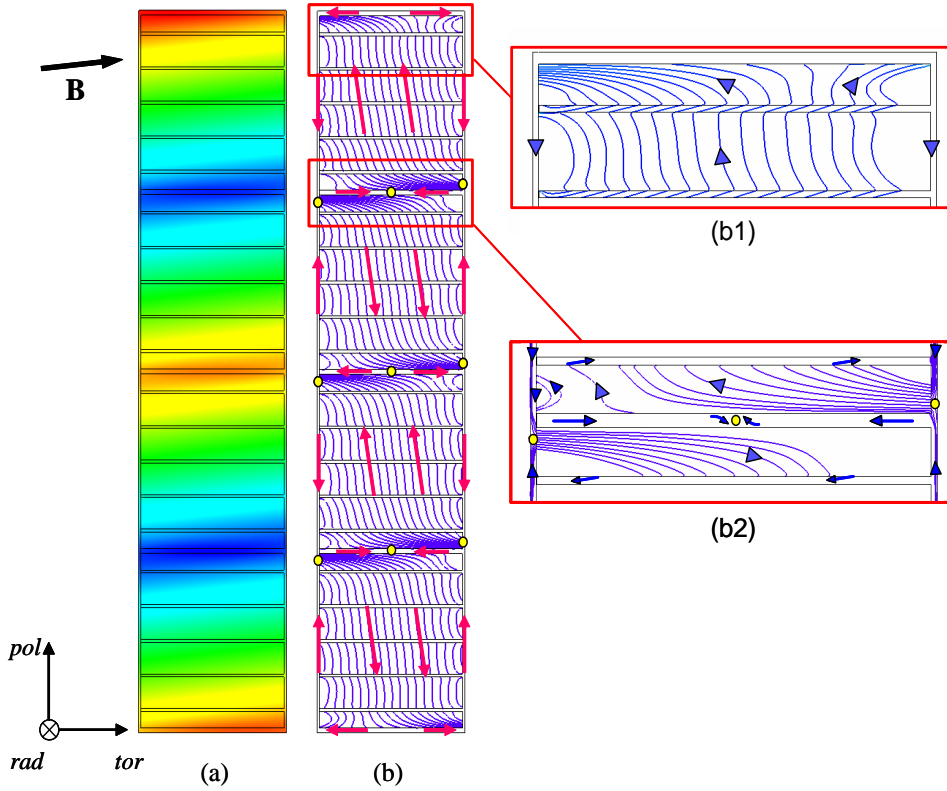


Figure 14: (a) Contour plots of the electric potential and (b) current streamlines for the case $B_{pol} = 0.1B_{tor}$, $Ha = 3000$. Some of the singular points created by the current vector field are marked by yellow dots.

The current distribution becomes more complex compared to the case of a pure toroidal magnetic field ($B_{pol} = 0$). As displayed in Fig.14b, a stronger exchange of currents occurs through the grid plates between adjacent breeder units, which corresponds to an intense electric coupling of the boxes.

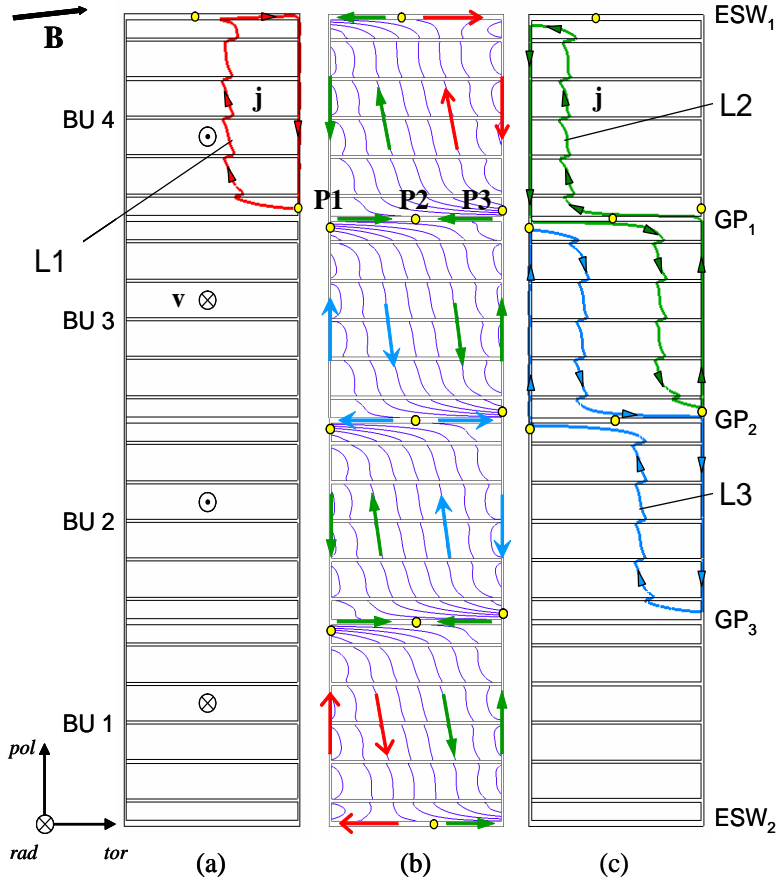


Figure 15: (b) Current streamlines in the four BUs for $Ha = 3000$ and $B_{pol} = 0.1B_{tor}$. Singularities created by the current vector field are marked by yellow dots (e.g. P1, P2, P3). (a) - (c) Characteristic current loops: path L1 closes in a single BU through the cooling plates; L2 and L3 connect electrically adjacent BUs.

The modified structure of the current paths can be described in terms of singularities created by the vector field of current density, highlighted by yellow dots in Figs.14-15. As mentioned before, in the case of a magnetic field aligned with the grid and cooling plates the critical points in the lateral walls of the mock-up are located at the intersection with the grid plates. In this case instead, when $B_{pol} \neq 0$, they are shifted along the poloidal direction in such a way that these points and the one in the center of the GP are aligned along a magnetic field line (e.g. P1, P2, P3 in Fig.15b). This displacement is related to the occurrence of current loops that connect different breeder units by crossing the common grid plate (paths L2 and L3 in Fig.15c). The presence of currents passing through the dividing wall is indicated by the fact that the current distribution around the singularity P2 at $z = 0$ is not symmetric with

respect to the toroidal and poloidal axes (compare Fig.5c, for $B_{pol} = 0$). In the two extreme boxes (BU 1 and 4), at the top and bottom of the mock-up, there are also current loops that do not cross the separating walls but couple electrically only the internal flat ducts (path L1 in Fig.15a).

5.2.2 Velocity

In Fig.16a the contour plot of the radial velocity is displayed in the cross section of the assembly.

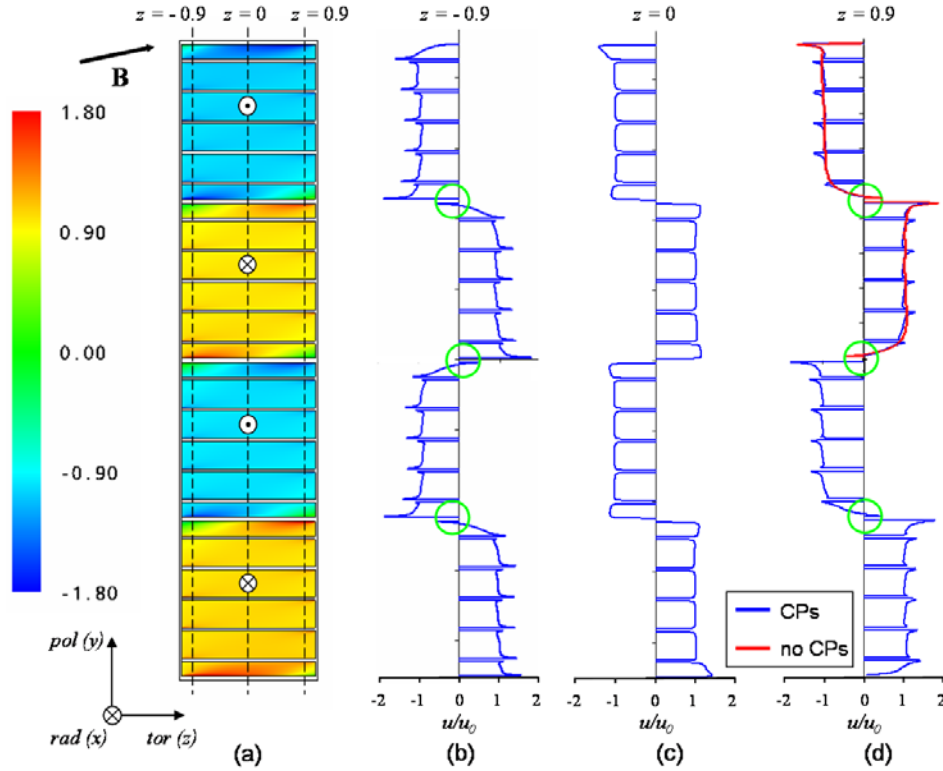


Figure 16: Radial velocity for $Ha = 3000$ and $B_{pol} = 0.1B_{tor}$. (a) Velocity contours and profile along the poloidal direction, (c) in the middle of the geometry ($z = 0$) and (b)-(d) close to the vertical walls ($z = \mp 0.9$). The green circles mark the zones with velocity reversed compared to the main stream and the red lines the results when omitting the CPs.

As a result of the presence of the poloidal component of the magnetic field, internal layers develop from the corners of the channels along magnetic field lines. This leads to a deformation of the velocity distribution compared to the case of pure toroidal magnetic field. The maximum value of the velocity close to GPs and ESWs is not localized any more at the symmetry plane ($z = 0$) but it is shifted towards the lateral walls. In Figs.16b-c-d the non dimensional radial velocity is plotted as a function of the poloidal coordinate along the line in the center of the geometry

at $z = 0$ and along those near the vertical walls at $z = \mp 0.9$. The velocity profiles show that in the middle of the breeder units a quite uniform distribution of the flow occurs. Instead, owing to the presence of cooling plates, close to the lateral walls there are regions where the velocity is locally increased. Moreover, in the breeder units a velocity reversed with respect to the main stream is observed in the corners next to the grid plates (as marked by the green circles in Figs.16b-d). This suggests the presence of closed recirculation loops in the flat sub-channels. The appearance of these regions is due to the electric flow coupling produced by the inclined magnetic field.

The red line in Fig.16d indicates the velocity profile in two BUs without internal cooling plates. A uniform flow distribution is present in the cores of the breeder units even close to the lateral walls. This case will be discussed later more in detail.

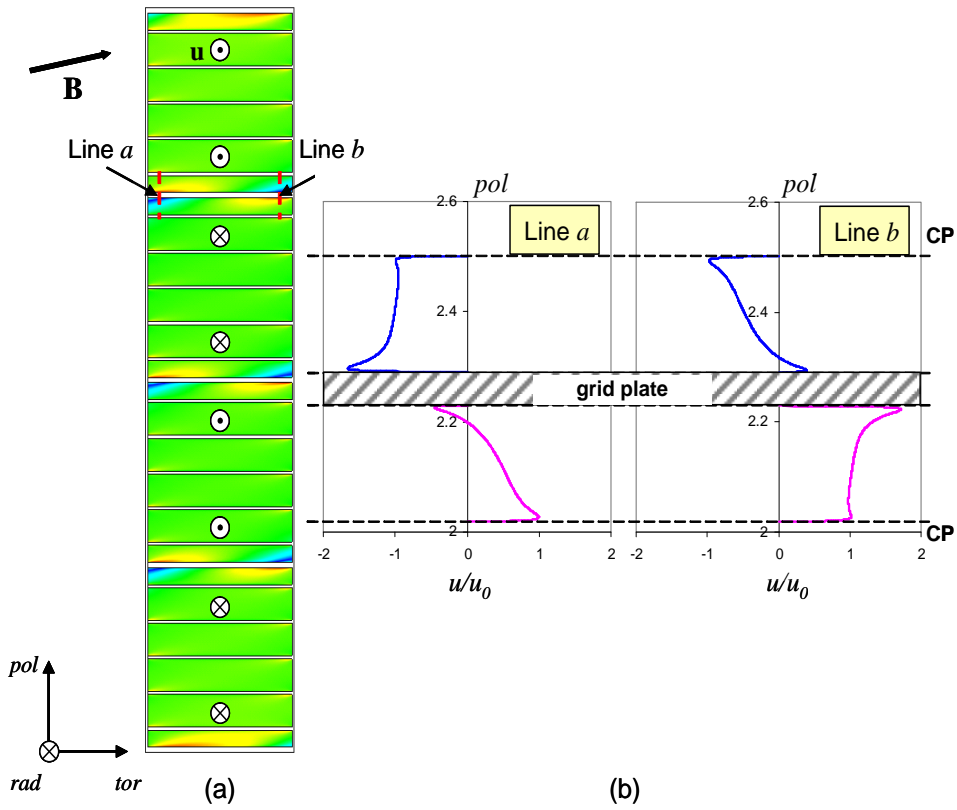


Figure 17: Radial velocity for $Ha = 3000$, $B_{pol} = 0.1B_{tor}$. (a) Contour plots of the magnitude of the radial velocity. (b) Non-dimensional velocity plotted as a function of the poloidal coordinate along the red dash lines (lines a and b). The fluid next to the grid plate, close to the vertical walls, moves in the same direction on both sides of the separating wall.

The described reverse velocity is displayed in Fig.17 where the enlarged detailed view shows the velocity profile in subdomains separated by a grid plate and belonging to two different BUs. The radial velocity is plotted along the red dash lines indicated

as line a and b in Fig.17a. It can be seen that the fluid close to the common plate, next to the vertical walls, moves in the same direction on both sides of the dividing plate although the driving pressure gradients and the mean flows are of opposite sign in these BUs.

This behavior can be further clarified by analyzing Fig.18. Here the red lines near the corners, at the grid plate, mark the locations where the velocity becomes zero ($\mathbf{u} = \mathbf{0}$). Each of these lines separates the region where the fluid moves according to the applied pressure gradient from the one where the velocity is reversed. Near the vertical walls the flow features are transferred from one breeder unit into the next one through the grid plates. This effect becomes more and more evident by increasing the poloidal component of the imposed magnetic field. The presence of this change of flow direction is related to the multichannel effect. In confirmation of that, at the external wall the liquid metal flows simply in the direction given by the driving pressure gradient.

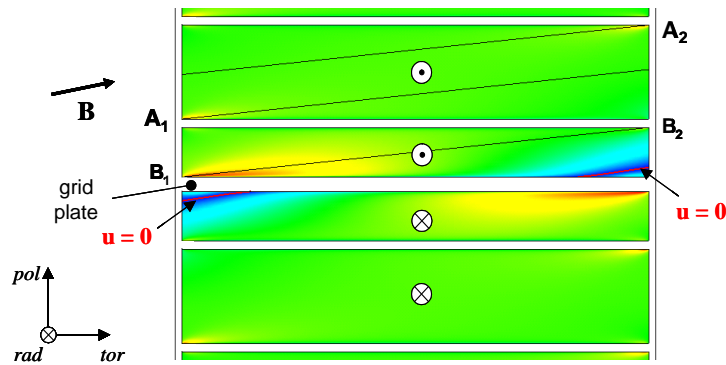


Figure 18: Contours of absolute velocity at the grid plate connecting two breeder units for $Ha = 3000$ and $B_{pol} = 0.1B_{tor}$. The red lines, close to the common wall, mark the locations where the velocity becomes zero. Each of these lines separates the region where the flow moves in the main stream from that with reversed flow. The black lines, aligned with the magnetic field, highlight the position of internal viscous layers.

In Fig.18 the black lines, which start from the points A_1 and A_2 , are aligned with the magnetic field and they indicate the location of internal viscous layers. Along these lines an increased value of the velocity is observed near the corners A_1 and A_2 . In the ducts at the top and bottom of a breeder unit, delimited on one side by the grid plate, there is in practice only one internal layer, whose position is indicated by the line B_1B_2 . This is due to the fact that, owing to the chosen inclination of the field and the larger aspect ratio of these channels compared with those between cooling plates, the two parallel layers originating from the duct corners combine forming a single region.

5.2.3 Current and velocity distribution without cooling plates

In order to understand the effects of the presence of the cooling plates on the flow distribution, the previous results are compared with those obtained when omitting these internal walls. Figure 19 shows the current streamlines in a breeder unit without cooling plates, for $B_{pol} = 0.1B_{tor}$ and $Ha = 3000$.

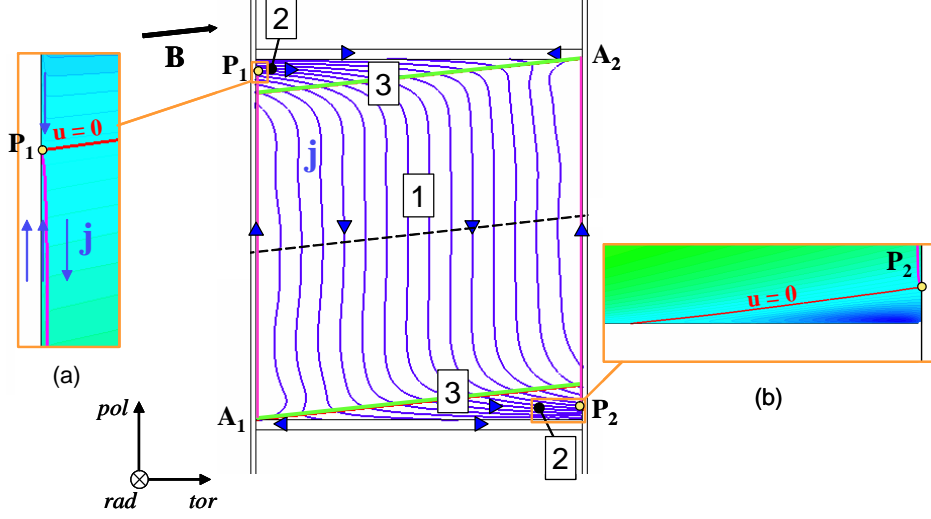


Figure 19: Current streamlines in a BU without cooling plates, for $Ha = 3000$ and $B_{pol} = 0.1B_{tor}$. The green lines are parallel to the imposed magnetic field and subdivide the BU in characteristic flow regions: (1) Hartmann-like flow with uniform core velocity and thin boundary layers. (2) Region where the velocity reduces and changes sign. (3) Internal layers aligned with \mathbf{B} where there are large gradients of flow variables.

The internal layers that develop from the duct corners (points A_1 and A_2) into the fluid along magnetic field lines subdivide the BU in 3 zones with defined features. In a range around these parallel layers, indicated by the green lines, strong gradients of the flow variables are present. The core region marked as 1 is characterized by current with uniform density that flows parallel to the vertical poloidal walls. By plotting the velocity along a line aligned with the magnetic field and passing through the center of the breeder unit (dash line), a Hartmann-like velocity profile is observed, with a homogeneous core distribution and thin boundary layers at the vertical walls. In these layers the velocity increases from zero at the wall to the constant value in the core region.

In Fig.19 the lines that develop along the poloidal direction starting from the characteristic points P_1 and P_2 mark the positions where the poloidal current component vanishes. They delimit the layer (Hartmann layer) in which part of the current induced in zone 1 closes its path. In these regions the current flows in reversed direction compared to the core stream (Fig.19a) and it is much larger. This is a typical behavior of the Hartmann flow. At points P_1 and P_2 the electric current

moves perpendicularly to the fluid-solid interface. In this area (region 2) there are currents coming from different breeder units (see Fig.15 for comparison). In zone 2, at the corners of the breeder unit close to P_1 and P_2 , the velocity decreases and inverts direction. Figure 19b shows the line along which the radial velocity component changes sign. In the triangle, at the duct corner, the fluid moves in direction opposite to that of the main stream imposed by the driving pressure gradient.

Figure 20 displays the velocity vector field for the discussed case and gives a global 3-D view of the flow structure. It shows that in the two central breeder units, at opposite corners with respect to the center of each box, the velocity has the same values and same direction. Because of the multichannel effect, along a grid plate, next to the vertical walls, the velocity has equal direction on both sides of the wall common to neighboring breeder units (Fig.20b).

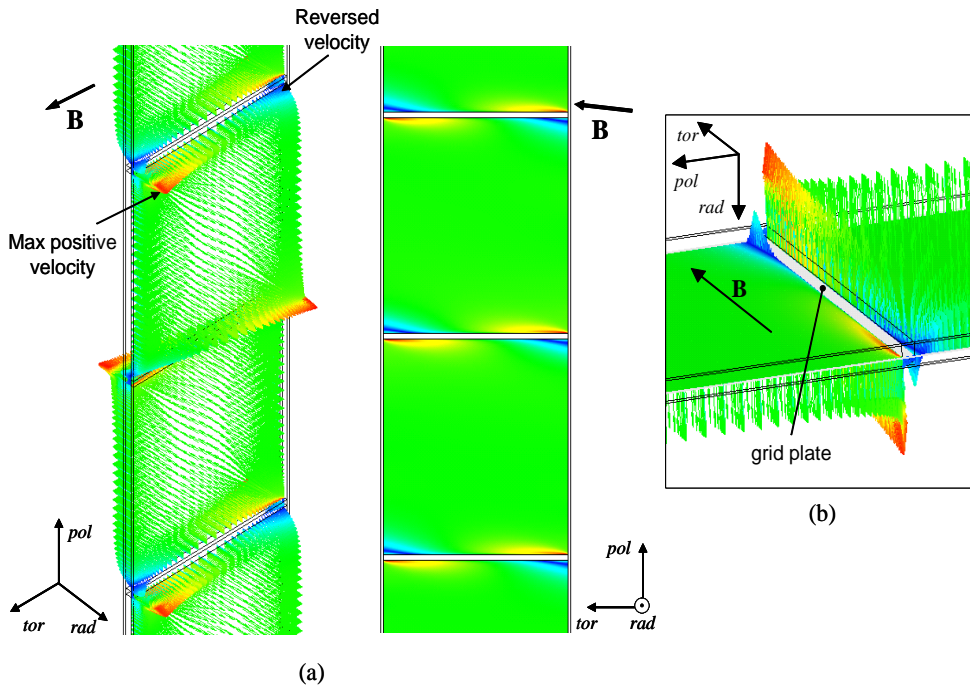


Figure 20: Velocity vector field in BUs without cooling plates, for $Ha = 3000$ and $B_{pol} = 0.1B_{tor}$. (b) Detailed view near a grid plate. Close to the walls parallel to the poloidal coordinate the velocity has the same direction on both sides of the common wall.

5.2.4 Effects of increasing the poloidal field component

Even if for applications in fusion technology it is expected that the poloidal component B_{pol} of the magnetic field, required to confine the plasma, is of the order of 10% of the toroidal one, results have been obtained also for larger values of B_{pol} in order to get a more complete picture of the multichannel effects that occur when a toroidal-poloidal magnetic field is applied.

In Figs.21-22 the electric potential and the velocity distribution are displayed in the four BUs for $Ha = 3000$ and two different inclinations of the magnetic field, $B_{pol} = 0.25B_{tor}$ and $B_{pol} = 0.5B_{tor}$, respectively. The red lines in Figs.21b-22b indicate the locations where the radial velocity becomes zero. These lines are almost aligned with the magnetic field. As in the previously discussed case ($B_{pol} = 0.1B_{tor}$), they subdivide the computational domain into areas such that, in each of them, the liquid metal moves in the same direction. The flow features are transferred from one fluid domain into the other through the cooling and grid plates. It is like having four channels with inclined walls, parallel to the applied \mathbf{B} . This effect becomes more and more evident by increasing the poloidal component of the magnetic field.

The locations where the red lines meet the external vertical walls correspond to the before-mentioned characteristic points in which the poloidal component of the current is zero. They mark the position where the currents coming from two different breeder units combine.

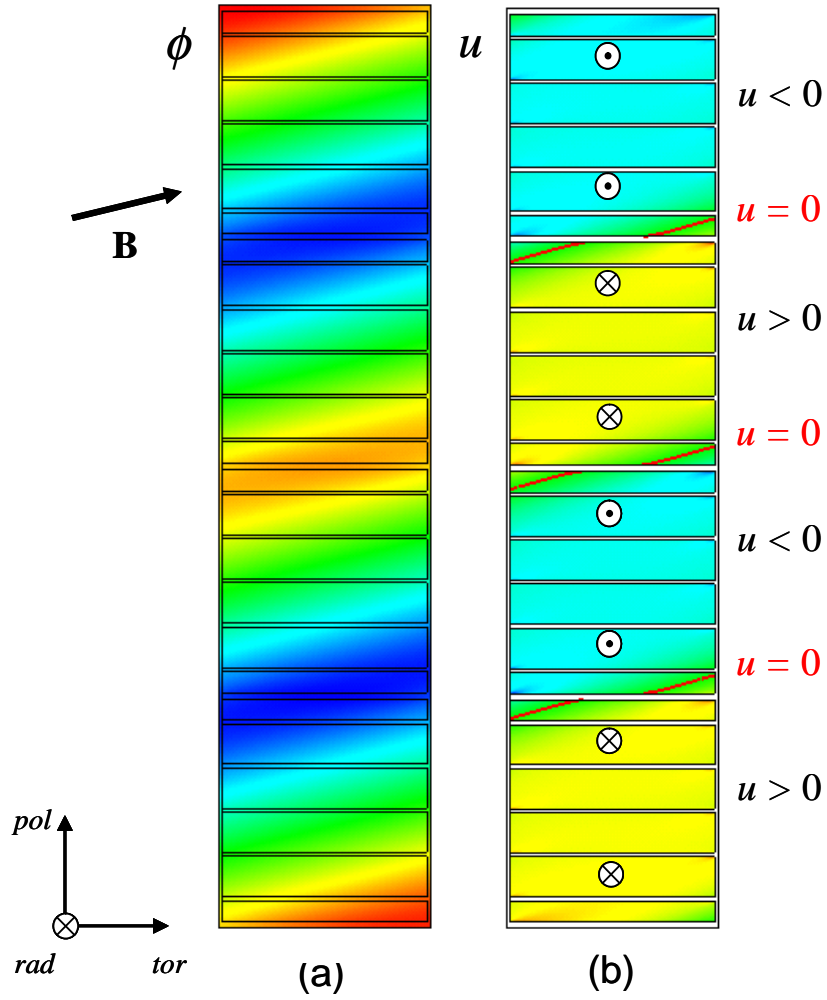


Figure 21: (a) Potential and (b) velocity distribution for $Ha = 3000$ and $B_{pol} = 0.25B_{tor}$. The red lines in (b) indicate the locations where the radial velocity changes sign. In each breeder unit the main flow direction, given by the driving pressure gradient, is indicated .

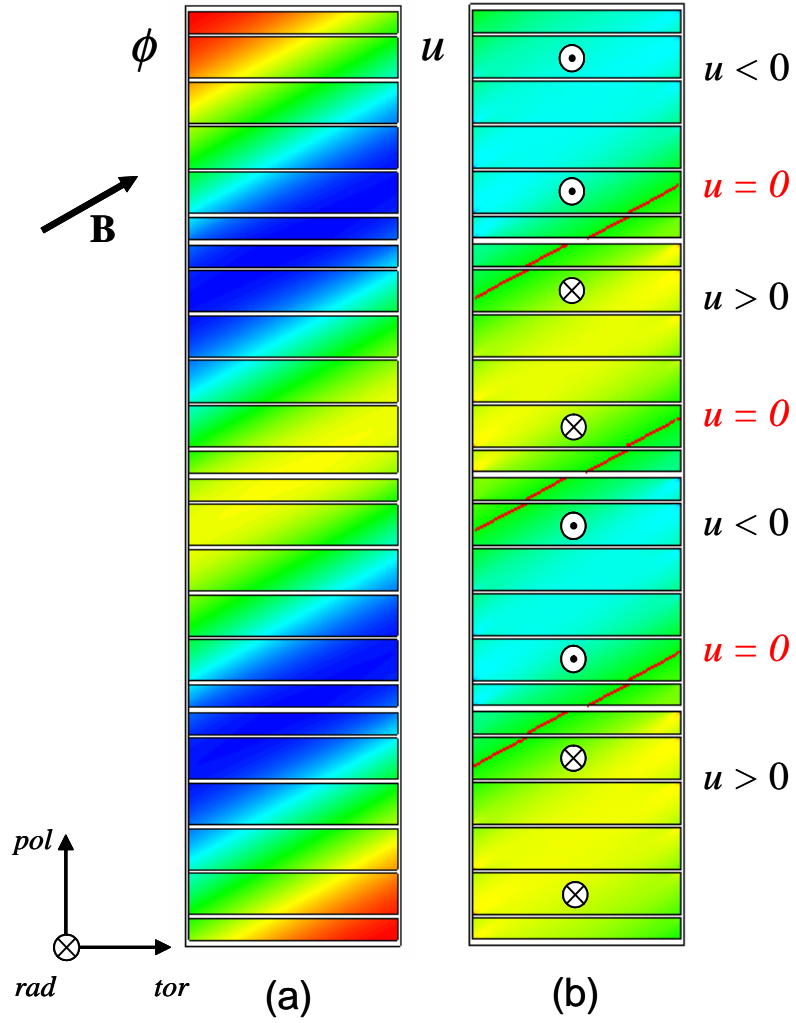


Figure 22: (a) Potential and (b) velocity distribution in four BUs for $Ha = 3000$ and $B_{pol} = 0.5B_{tor}$. The red lines in (b) indicate the positions where the radial velocity vanishes.

5.3 Poloidal magnetic field

Let us consider the MHD flows in 4 BUs exposed to a purely poloidal magnetic field ($\mathbf{B} = B_{pol}\hat{\mathbf{y}}$). The breeder units and the internal sub-channels are coupled at the walls perpendicular to the magnetic field, called the Hartmann walls. This limiting case has been investigated to support the discussion concerning a possible modification of the present HCLL blanket design by rotating the breeder units by 90° degrees. In that case grid and cooling plates would be perpendicular to the main field component.

Questions about improvements and modifications of the present design are still open, and therefore it is interesting to understand the behavior of the flow in the breeder units when a different orientation of the blanket modules is assumed.

In order to describe the main features of the MHD flow when a poloidal magnetic field is applied, first for simplicity the results for the case without internal cooling plates are discussed. The calculations have been performed by forcing the same flow rate in the four breeder units, imposing appropriate driving pressure gradients. All the following observations aim to give a general understanding of the particular flow under study.

5.3.1 Electric potential and current density

Figure 23(a) shows the contours of the electric potential in the cross section of the assembly for $Ha = 3000$ and $\mathbf{B} = \hat{\mathbf{y}}$. In each breeder unit the main flow direction, as expected according to the driving pressure gradient, is also indicated. In Fig.23c the potential is plotted as a function of the toroidal coordinate z , along the lines in the center of each breeder unit marked as dash lines in Fig.23a. These profiles highlight the symmetric distribution of the potential with respect to the plane $z = 0$, along which the cancellation of ϕ is observed. Moreover, it can be noted that the transverse potential gradient $\partial\phi/\partial z$ is linear in the duct core. Instead, when approaching the side walls, it deviates from this linear trend and it increases. As mentioned above, along magnetic field direction the potential variation is zero on the *rad-pol* symmetry plane $z = 0$ and it becomes larger near the side walls. Here the potential difference across the grid plates drives current through these Hartmann walls. This gives rise to the current distribution shown in Fig.23b. Typical current paths are displayed in different colors. Due to the reverse pressure gradient in adjacent ducts the current in the cores is induced in opposite direction. The major fraction of the current tends to flow towards the walls parallel to the magnetic field, the side walls, creating large current loops that bypass and enclose the common separating grid plate, as shown by the current streamlines highlighted in green and yellow. Current induced in the cores turns into the side layers and into the parallel walls and it is transferred from one breeder unit into the adjacent one short circuiting the grid plates. The largest values of current density are present at the intersection between grid plates and side walls. In Fig.23b the yellow dots mark the location of characteristic points of the current vector fields. Around them the current induced in one breeder unit splits into two parts that move in opposite poloidal direction. In the

case of the central units it means that these two portions of current are transferred towards different neighboring breeder units.

The resulting strong electric coupling with the variation of current density along magnetic field direction in the region close to the side walls represents a source of flow vorticity. This latter modifies substantially the velocity distribution compared to that in a single separated duct.

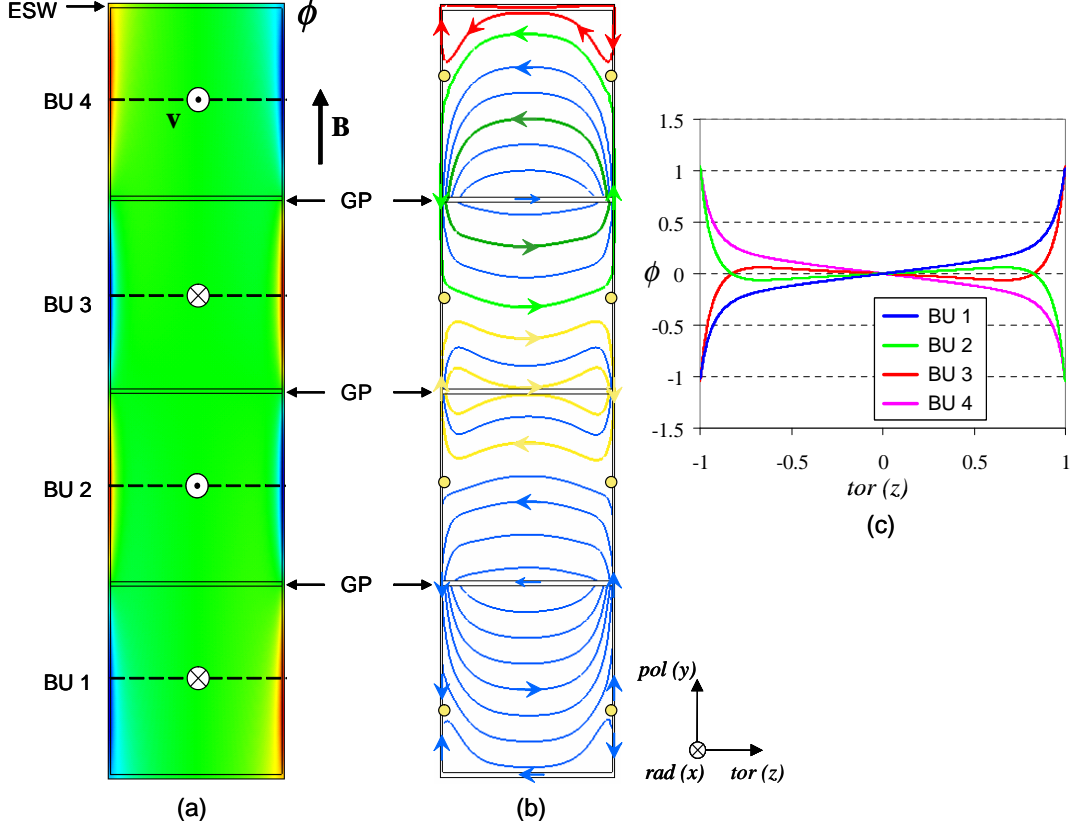


Figure 23: (a) Contours of the electric potential. In each unit the direction of the main flow is marked. (b) Current streamlines and characteristic loops in the four breeder units. (c) Potential profiles as a function of the toroidal coordinate z along the dash lines in (a), in the middle of each breeder unit. Results for $Ha = 3000$ and $\mathbf{B} = \hat{y}$.

Calculations have been also performed including the cooling plates in the breeder units. It has been observed that the presence of the internal plates determines a deformation of the current paths since the current tends to turn inside the cooling plates instead of following a straight way inside side walls and boundary layers. Nevertheless, the main features of the current density distribution remain similar to those described for the case in which the cooling plates are omitted.

5.3.2 Velocity

Figure 24a shows qualitatively the velocity distribution in the blanket mock-up for $Ha = 3000$ and $\mathbf{B} = \hat{y}$. As a result of the electric flow coupling of the fluid domains, in the center of the BUs there is almost no flow. This reduced flow rate could lead to high tritium concentration and to an increase of its permeation towards the helium channels integrated in the cooling plates.

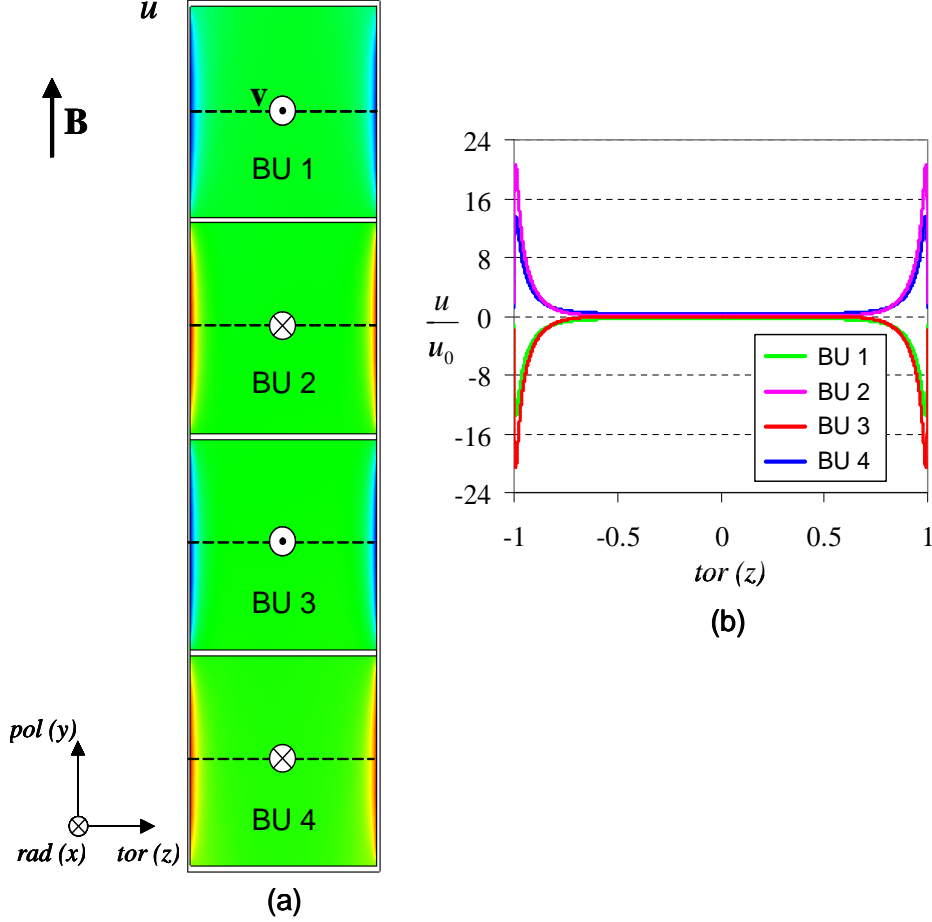


Figure 24: (a) Contours of the velocity in the cross section of breeder units. Maximum values occur at the side walls parallel to the magnetic field. (b) Velocity profiles along toroidal direction, in the center of each BU. Results for $Ha = 3000$ and $\mathbf{B} = \hat{y}$.

Instead along side walls, parallel to the magnetic field, strong velocity jets are present as illustrated in Fig.24b where the non dimensional velocity is plotted as a function of the toroidal coordinate along the dash lines in the middle of each breeder unit. It can be observed that in the two external boxes (BU 1 and BU 4) the fluid moves according to the direction imposed by the applied body force. On the contrary in the two internal units (BU 2 and BU 3) the liquid metal flow in the cores is reversed and moves in the same direction as the fluid in the adjacent external box even if driven by opposite pressure gradient. In other words the extreme breeder

units "pull the fluid of the adjacent box in their own direction". Nevertheless the value of the velocity in the cores of BU 2 and BU 3 is almost zero. Near the side walls instead the flow occurs in the expected direction. The flow distribution in the two central breeder units recalls some of the characteristics of flows in ducts with perfectly conducting Hartmann walls as investigated by Hunt (1965), where the core is almost stagnant and all the fluid is carried by the side layers.

6 Comparison with experimental data

Numerical results have been compared with data obtained from the experiments performed in the MEKKA laboratory at the Forschungszentrum Karlsruhe.

Figure 25 shows the instrumented experimental test section positioned in front of the magnet. The insulating green plates that cover the walls of the mock-up are supplied with spring-loaded probes for measurements of surface electric potential. The data acquisition system for potential data consists basically of a 600 channel low noise ($< 1 \mu\text{V}$) relay multiplexer and a very sensitive voltmeter (resolution 10 nV). The measuring time for each potential value was in the range of 2 s.

The measured values that are used for the comparison with the numerical results are those recorded on the Hartmann wall, i.e. the wall perpendicular to the magnetic field, in the central radial position $x = 0$, at half distance from back plate and first wall (dash line in Fig.25). This is the only radial location at which all the four breeder units are completely instrumented with potential sensors. For the other positions instead only the Hartmann walls of units 3 and 4 of the experimental mock-up are homogeneously covered by potential electrodes. An array of more than 200 sensors is used to record the potential distribution on these walls. On the Hartmann wall of the other two breeder units only few sensors are present and the values recorded at those points should allow checking the assumed symmetry in the poloidal distribution of the electric potential. It should be noticed that perfect symmetry conditions with respect to the middle grid plate that separate BU 2 and 3 are expected only in the inertialess regime, i.e. for small velocities (very large interaction parameter - small Reynolds number).

Figure 26 displays the contours of measured electric potential on the surface of the mock-up. Since the electric potential may serve as an approximate stream function of the flow, lines of constant potential, i.e. with the same color, represent velocity streamlines. Therefore, the fluid inside the test section tends mainly to follow lines of constant color. The experimental data show that, for strong magnetic fields, in the central part of the test section, i.e. in the *rad-pol* plane marked in the figure by the dash lines, fully developed conditions are present. This justifies the assumption of fully developed flow used in the calculations discussed in the present report.

It has been also found that the strongest 3D MHD effects appear at the junction between circular pipes and manifolds as well as when the liquid metal enters the breeder unit and expands from the manifold into the larger box. Similar phenomena are observed when the working fluid NaK leaves the breeder units to be collected into the draining manifold (Starke, Bühler and Horanyi (2008)).

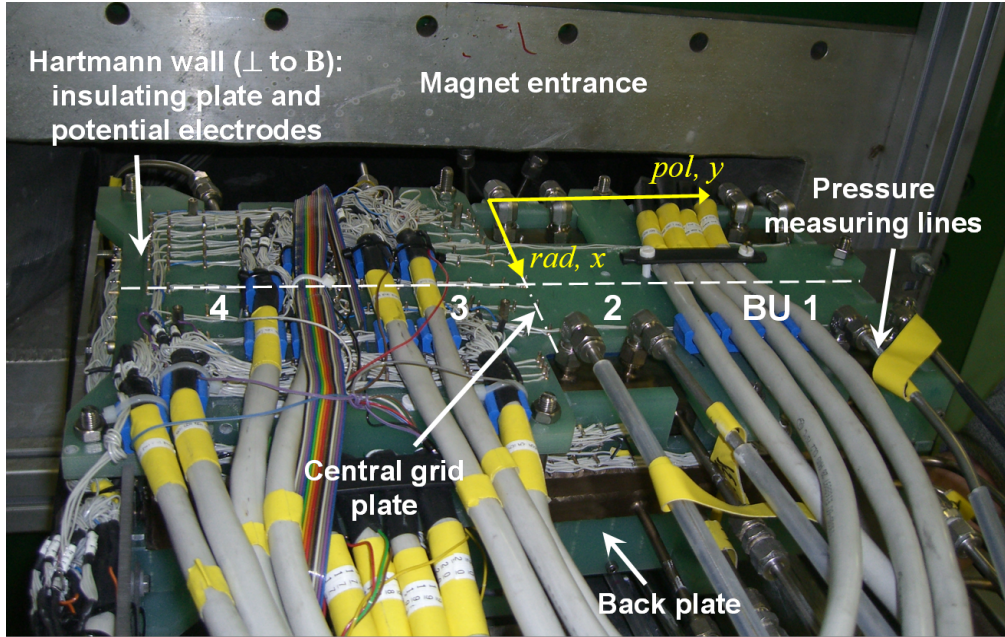


Figure 25: View on the experimental test section in front of the magnet. The green insulating plate on the Hartmann wall is covered by an array of 200 electrodes for recording electric potential distribution. The back plate, where the manifolds are located, is shown in the foreground.

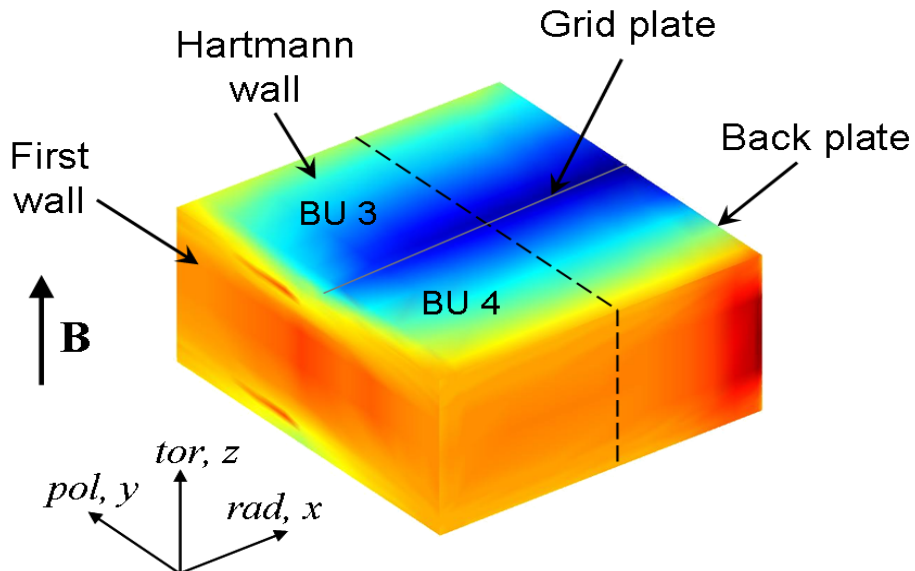


Figure 26: Measured contours of electric potential on the Hartmann wall of breeder units 3 and 4 for $Ha = 3000$ and $N = 1325$. The recorded potential profile on the Hartmann wall, along the poloidal dash line, is compared with the numerical results.

In Fig.27 the calculated electric potential for $Ha = 3000$ is plotted as a function of the poloidal coordinate along the Hartmann wall of the test section. The results are compared with experimental data obtained for various Reynolds numbers. The comparison shows a good agreement confirming that the used instrumentation is suitable for recording the potential distribution on the surface of the mock-up and hence getting reliable indications about the flow inside. The small deviations between numerical and experimental values can have different reasons. For instance imperfections in the manufactured test section, e.g. non homogeneous wall thicknesses and variations with respect to the original technical drawings. This results in non uniform electric conductance of the walls with consequent effects on potential and flow distribution in the mock-up. Inertia effects can also lead to deviations from the assumed fully developed conditions in the center of the geometry, even if in the present case, for the shown Reynolds numbers, almost no effect of inertia forces is observed. This influence is instead clearly evident when smaller magnetic fields, i.e. smaller Hartmann numbers, are considered in the experiments. Moreover, it can be observed that the agreement is better for the data recorded on breeder units 3 and 4 ($y < 0$). This could be due to the fact that on the surface of the boxes 1 and 2 there are the pressure taps that can disturb the reading of the potential sensors and affect the flow distribution by creating additional current paths. A detailed description of the experimental results is given in Bühler et al. (2008).

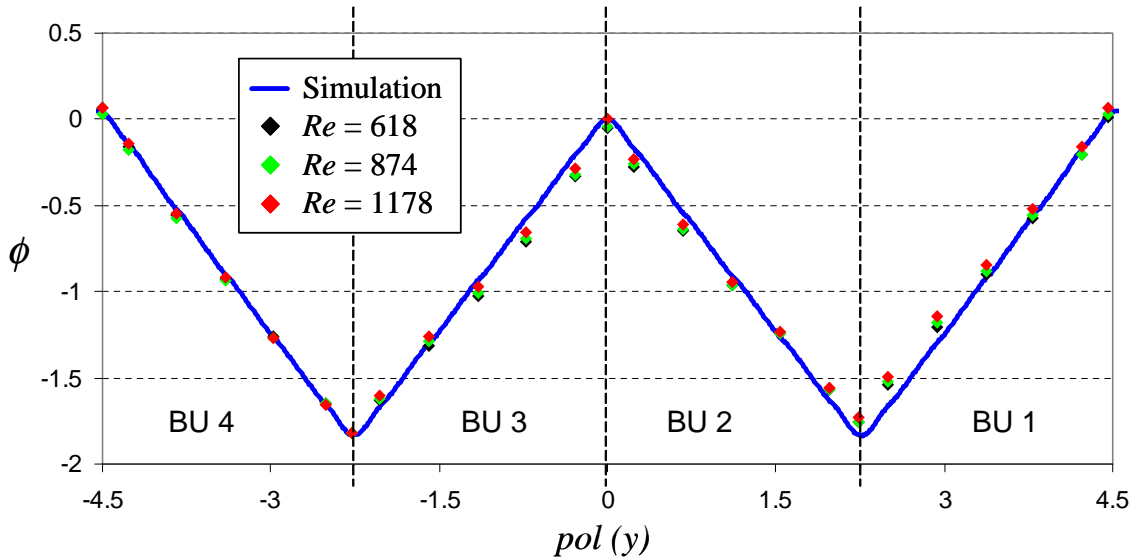


Figure 27: Potential profile along the Hartmann wall of the assembly for $Ha = 3000$. The numerical results are compared with experimental data obtained for different Reynolds numbers.

7 Conclusions

A helium cooled lead lithium blanket concept has been proposed to be tested during ITER operation as part of the European fusion program.

An experimental campaign aiming to analyze the MHD flow features in such a design and to qualify its performance is currently under development at the Forschungszentrum Karlsruhe. Due to the limited volume of homogeneous magnetic field available in the magnet used for the experiments, the size of the test section reproduces those of the original design scaled by a factor two.

A combination of experimental data, numerical results and extrapolated correlations will be used to predict flow and pressure distribution in the HCLL blanket modules in a wide range of characteristic parameters and to suggest suitable improvements and modifications.

As a complement and support to the experimental program, a numerical study has been performed, where fully developed MHD flows in four breeder units, each containing five cooling plates, have been investigated. The geometry is chosen according to the features of the manufactured test section. The numerical analysis focuses on the description of velocity, potential and current distributions in the breeder units, by evaluating the effects of full electrical coupling of the flow in the 24 fluid domains depending on the applied magnetic field. Different cases have been considered: by starting from a pure toroidal magnetic field an additional poloidal component has been added and progressively increased.

In the case of a toroidal magnetic field the currents induced in the cores of the channels formed between cooling plates cross these internal side walls mainly perpendicularly and couple strongly the flat sub-channels. This leads to a quite uniform flow distribution among cooling plates. The velocity profile in the slender ducts having same aspect ratio resembles the one in a duct with perfectly conducting side walls. It is characterized by a uniform core velocity and a slight increase at the walls parallel to the magnetic field. Instead, in the internal grid plates that separate adjacent breeder units and in the external side walls the currents flow preferentially in tangential direction. As a result an increased velocity appears at these side walls. The flow rate is slightly smaller near the external side walls compared to the one at the grid plates due to the larger effective wall conductance of the former ones. The MHD velocity distribution with increased flow rate at the walls dividing the blanket into breeder units can be regarded as a positive feature, since high flow rates at the separating walls are desirable to keep tritium losses within acceptable values. A grid sensitivity study showed that the maximum velocity near the grid plates and the external side walls could even increase by inserting additional nodes in the parallel layers. This possibility cannot be considered at the present time due to limitations in computational resources.

It can be also noted that no exchange of current occurs between breeding boxes, corresponding to a weak electric coupling of the four units. This condition is the result of combined and concomitant factors: the particular flow arrangement given by the design, characterized by counter-current flows at the common grid plates and co-current flow among cooling plates, the applied magnetic field parallel to grid and

cooling plates.

When an additional poloidal component of the imposed magnetic field is taken into account, internal layers develop in the fluid along magnetic field lines, starting from the corners of the ducts. Inside these layers there are strong gradients of flow variables. They subdivide the flow domain in various regions with specific features and lead to a modification of the flow distribution in the breeder units that depend on the value of the poloidal component of \mathbf{B} . More specifically, due to the presence of the internal layers, the solutions for velocity and electric potential are aligned with the imposed magnetic field. Moreover, zones with velocity reversed with respect to the main stream direction given by the applied driving pressure gradient appear in the breeder units, near the grid plates. For a sufficiently large poloidal component the solution seems to ignore the presence of the internal walls and the flow features are "transferred" from one fluid domain into the others through the plates. In other words, it is like having four units with inclined walls that are parallel to the magnetic field.

Since there are still open questions about possible modifications of the proposed HCLL design, like for instance the idea of turning the blanket modules by 90° , in the present numerical analysis also the limiting case of a pure poloidal magnetic field has been investigated. It has been found that the internal walls perpendicular to the magnetic field, i.e. the grid plate act as a short cut for the breeder units. As a result, the flow in the fluid domains is strongly coupled, the major part of the flow is carried by the side layers that develop at the walls parallel to \mathbf{B} and the cores are almost stagnant. This flow distribution would not ensure the minimum core flow rate required for tritium removal and purification of the liquid metal. Moreover, the high velocity jets at the side walls, even if they could be useful to reduce tritium permeation into the helium channels embedded in the walls, they could cause an increase of corrosion rates probably up to unacceptable values. In addition, a very high pressure drop could occur. Therefore, this orientation of the blanket modules is not recommended.

The calculated poloidal profile of electric potential on the Hartmann wall for the case of toroidal magnetic field has been compared with experimental data. A good agreement has been found, confirming the validity of the employed measuring techniques and the possibility of using the recorded surface potential for getting reliable information about the flow inside the mock-up. For instance, at the Hartmann wall, on the symmetry plane $z = 0$ of the test section, for high Hartmann numbers, the measured potential shows that an almost constant gradient is present across the breeder units, indicating a uniform flow partitioning among the electrically coupled sub-channels. Moreover, for strong magnetic fields, the experiments confirm the existence of a fully developed flow region in the center of the breeder units at half distance from the back plate and the first wall as assumed in the simulations. A detailed description of the experimental results is given in Bühler et al. (2008).

8 Further required investigations

In the case of a pure toroidal magnetic field, namely when the magnetic field is parallel to grid and cooling plates, side layers form at all the walls aligned with \mathbf{B} . For fusion relevant conditions, i.e. in the case of strong magnetic fields (large Hartmann numbers Ha), it could be interesting to verify the presence of instabilities that can generate local turbulence and affect mass and heat transfer processes.

Since in the real geometry tolerances for the thickness of the walls have to be considered, it would be necessary to investigate the effects of the variation of wall thickness and therefore of the effective electrical conductance on velocity and current distribution in the breeder units. Moreover, in the original blanket modules, helium channels are present in all the walls. Their presence determines a particular current distribution in the walls and a non uniform electrical conductance, whose effects on the flow characteristics have to be analyzed.

In the discussed numerical results a single column of breeder units has been considered. Nevertheless, a complete blanket module is formed by a number of columns one adjacent to the other. Therefore, a second kind of electric flow coupling should be studied that takes into account, in the case of toroidal magnetic field, the connection of columns of breeder units through the Hartmann walls perpendicular to the magnetic field

Additional calculations are foreseen for larger Hartmann numbers to further approach the fusion conditions.

References

- Barleon, L., Mack, K.-J. and Stieglitz, R.: 1996, The MEKKA-facility - A flexible tool to investigate MHD-flow phenomena, *Technical Report FZKA 5821*, Forschungszentrum Karlsruhe.
- Boccaccini, L., Giancarli, L., Janeschitz, G., Hermsmeyer, S., Poitevin, Y., Cardella, A. and Diegele, E.: 2004, Materials and design of the European DEMO blankets, *Journal of Nuclear Materials* **329-333**, 148–155.
- Bühler, L.: 2005, Magnetohydrodynamic pressure-driven flows in the HCLL blanket, *Fusion Engineering and Design* **75-79**, 923–926.
- Bühler, L., Brinkmann, H.-J., Horanyi, S. and Starke, K.: 2008, Magnetohydrodynamic flow in a mock up of a HCLL blanket. Part II Experiments, *Technical Report FZKA 7424*, Forschungszentrum Karlsruhe.
- Foust, O. J.: 1972, *Sodium - NaK engineering handbook*, Gordon and Breach Science Publishers.
- Hunt, J. C. R.: 1965, Magnetohydrodynamic flow in rectangular ducts, *Journal of Fluid Mechanics* **21**, 577–590.
- McCarthy, K. A. and Abdou, M. A.: 1991, Analysis of liquid metal MHD flow in multiple adjacent ducts using an iterative method to solve the core flow equations, *Fusion Engineering and Design* **13**, 363–380.
- Mistrangelo, C.: 2005, *Three-dimensional MHD flow in sudden expansions*, PhD thesis, Universität Karlsruhe.
- Molokov, S.: 1993, Fully developed liquid-metal flow in multiple rectangular ducts in a strong uniform magnetic field, *European Journal of Mechanics, B/Fluids* **12(6)**, 769–787.
- Morley, N. B., Malang, S. and Kirillov, I.: 2005, Thermofluid magnetohydrodynamic issues for liquid breeders, *Fusion Science and Technology* **47(3)**, 488–501.
- Patankar, S. V.: 1980, *Numerical Heat Transfer and Fluid Flow*, Hemisphere Publ.Co.
- Rampal, G., Gatelet, D., Giancarli, L., Laffont, G., Li-Puma, A., Salavy, J. and Rigal, E.: 2006, Design approach for the main ITER test blanket modules for the EU helium cooled lithium-lead blankets, *Fusion Engineering and Design* **81**, 695–700.
- Rampal, G., Li-Puma, A., Poitevin, Y., Rigal, E., Szczepanski, J. and Boudot, C.: 2005, HCLL TBM for ITER - design studies, *Fusion Engineering and Design* **75-79**, 917–922.

Starke, K., Bühler, L. and Horanyi, S.: 2008, Experimental investigations of liquid-metal MHD flows in a mock-up of a helium cooled lead-lithium test blanket for ITER, *Proceedings of the 7th Pamir International Conference, Presq'île de Giens, France September 8-12*. To be published.